Microwave-assisted Synthesis of Modified Cyclopentadienyl Iridium and Rhodium Chloro-bridged Dimers

Loren Christopher Brown

Thesis submitted to the faculty of the Virginia Polytechnic Institute and State University in partial fulfillment of the requirements for the degree of

Master of Science

In

Chemistry

Joseph S. Merola, Chair

John R. Morris

Gordon T. Yee

Blacksburg, VA

Keywords: iridium; rhodium; tetramethylcyclopentadiene; microwave; dimer; diene; crystal structure; diol; lactone

Microwave-assisted Synthesis of Modified Cyclopentadienyl Iridium and Rhodium Chloro-bridged Dimers

Loren Christopher Brown

Abstract

The present work describes the design and synthesis of a series of dimers $[(\eta^5\text{-ring})MCl]_2(\mu^2\text{-}Cl)_2$, (where $(\eta^5\text{-ring})MCl$ = $(\eta^5\text{-}Me_4C_5R)Rh(III)Cl$ or $(\eta^5\text{-}Me_4C_5R)Ir(III)Cl$). Iridium and rhodium dimeric complexes were synthesized via a microwave reaction and directly compared through single-crystal X-ray crystallography. Finally, the dimeric complexes were evaluated as potential oxidation catalysts.

The modified HCp^{*R} (R = isopropyl, *n*-butyl, isobutyl, *sec*-butyl, *n*-pentyl, *n*-hexyl, *n*-heptyl, *n*-octyl, phenyl, benzyl, phenethyl, cyclohexyl, and cyclopentyl) type ligands were synthesized by reaction of 2,3,4,5-tetramethylcyclopent-2-en-1-one with the respective Grignard reagent (RMgX), followed by elimination of water under acidic conditions to produce the tetramethyl(alkyl or aryl)cyclopentadienes in moderate to excellent yields (39 - 98%). Reaction of the HCp^{*R} ligands with $[M(COD)](\mu^2\text{-}Cl)_2$ (M = Rh, Ir; COD = 1,5-cyclooctadiene) gave the dimeric complexes $[Cp^{*R}MCl]_2(\mu^2\text{-}Cl)_2$ in yields ranging from 16 - 96%. The dimers were characterized by nuclear magnetic resonance (NMR) spectroscopy, single-crystal X-ray diffraction (XRD) (supplemented by powder XRD), high-resolution mass spectrometry (HRMS), and elemental analysis. Complexes studied by XRD were analyzed to understand the bond lengths and bond angles throughout each complex. The dimeric complexes synthesized, will facilitate a complete study on how the R group influences catalytic activity.

Acknowledgements

I would like to thank Emily Ressegue who helped with the syntheses of these compounds.

I would like to thank Chrissy DuChane for her assistance with biological testing, encouragement, and countless hours of proofreading.

I would like to thank Dr. Paul Deck for his assistance with proofreading and support.

I would like to thank Bryce Kidd and Chris Houser for their assistance in proofreading.

I would like to thank Dr. Gordon Yee and Dr. John Morris for serving as my committee members.

I would like to thank both Dr. Carla Slebodnick and Dr. Elinor Spencer for their guidance and assistance with crystallography.

I would like to thank my advisor, Dr. Joseph Merola, for his guidance, encouragement, and resounding support.

Abbreviations

ADP = Anisotropic displacement parameters

Bn = Benzyl

$CDCl_3$ = Chloroform-*d*

COD = 1,5-Cyclooctadiene

Cp* = Pentamethylcyclopentadienyl ligand

Cyh = Cyclohexyl

Cyp = Cyclopentyl

DCM = Dichloromethane

EDG = Electron donating group

EWG = Electron withdrawing group

Hex = Hexanes

MeOH = Methanol

Ph = Phenyl

RBF = Round bottom flask

SiO_2 = Silica gel

Chapter 1 Introduction

1.1 Importance of iridium and rhodium dimers

Rhodium and iridium dimers of the type $[Cp^*MCl]_2(\mu^2\text{-}Cl)_2$ (M = Rh, Ir) are employed in various catalytic systems[1,2] and are useful synthetic precursors in half-sandwich chemistry.[3] Rhodium and iridium Cp* compounds are synthesized in yields of 95% and 85%, respectively, by the reaction of the metal trichlorides with pentamethylcyclopentadiene.[4] The investigation of cyclopentadienyl ligands is of significant importance due to the ease with which their steric and electronic properties can be altered;[5] however, modified variants of Cp* groups have rarely been investigated. Morris *et al.*, Sadler *et al.*, and Dooley *et al.* have demonstrated that the synthesis of modified Cp* iridium dimeric complexes proceeds with low yields, 40 - 57%, 39%, and 16% respectively.[6-7] Consequently, the synthesis of dimeric noble metal derivatized-cyclopentadienyl complexes is in need of improvement.

Catalytic applications of the metal dimers include N-alkylation of amines,[8] N-heterocyclization of primary amines with diols,[9] functionalization of aromatic C-H bonds,[10] and alkyne hydroamination to 1,2-dihydroquinolines,[11] among others.[12] More commonly, rhodium and iridium dimers have been explored in numerous oxidative catalytic systems. Fujita *et al.* investigated both iridium and rhodium pentamethylcyclopentadiene dimers for the oxidation of secondary alcohols under mild conditions to provide a safer alternative to toxic chromium reagents.[13] Though most hydrogen transfer oxidations are studied for secondary alcohols, Fujita also examined the use of $[Cp^*MCl]_2(\mu^2\text{-}Cl)_2$ for the oxidation of primary alcohols. In the conversion of alcohols to aldehydes (**Figure 1**), $[Cp^*IrCl]_2(\mu^2\text{-}Cl)_2$ was found to have greater activity than the rhodium analogue.[13] Results for the oxidation of various primary alcohols by $[Cp^*IrCl]_2(\mu^2\text{-}Cl)_2$ are shown in **Table 1**. In this study, benzyl alcohol was converted to

benzaldehyde (87% yield); these results are improved when there is an electron donating group (EDG) in the para position of the benzyl alcohol as evidenced by entries 2 and 3, and decreased with an electron withdrawing group (EWG) in the para position (Entries 7 and 8). Conversion of the alcohol decreased when the EDG was in the ortho position. In comparison to primary alcohols, secondary alcohols were found to be easier to oxidize (**Table 2**).

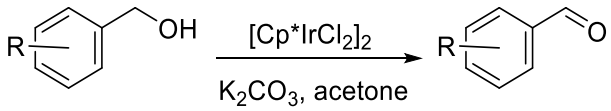

Figure 1. General scheme for the oxidation of primary alcohols to aldehydes.

Table 1. Oxidation of primary alcohols to aldehydes catalyzed by $[Cp^*IrCl]_2(\mu^2\text{-}Cl)_2$.[a]

Entry	Alcohol	Conv. Of alcohol (%)[b]	Yield of aldehyde (%)[b,c]
1	benzyl alcohol	87	87(74)
2	*p*-Me	100	93(82)
3	*p*-OMe	100	99(90)
4	*o*-OMe	70	67(63)
5	*m*-OMe	85	85(77)
6	*p*-OH	77	60
7	*p*-Cl	72	70(61)
8	*p*-NO_2	32	20

[a] Performed at room temperature for 6 h with corresponding alcohol (1.0 mmol), $[Cp^*IrCl]_2(\mu^2\text{-}Cl)_2$, (2.0 mol% Ir) and K_2CO_3 (0.10 mmol) in acetone (30 mL). [b] Determined by GC based on the starting alcohol. [c] The value in parentheses is the isolated yield.[13]

Table 2. Oxidation of secondary alcohols to ketones catalyzed by $[Cp^*IrCl]_2(\mu^2\text{-}Cl)_2$.[a]

Entry	Alcohol	Conv. Of alcohol (%)[b]	Yield of ketone (%)[b,c]
1	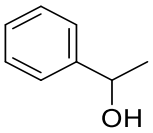	100	100(94)
2	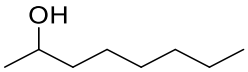	89	88(77)
3	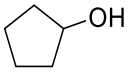	100	100
4	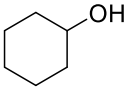	79	79

[a] The reaction was performed at room temperature for 6 h with secondary alcohol (2.0 mmol), $[Cp^*IrCl]_2(\mu^2\text{-}Cl)_2$, (0.5 mol% Ir) and K_2CO_3 (0.20 mmol) in acetone (2 mL). [b] Determined by GC based on the starting alcohol. [c] The value in parentheses is the isolated yield.[13]

The mechanism for this reaction involves the formation of a metal-alkoxide (**1**, **Figure 2**) followed by the release of the product via β-hydride elimination, forming a metal hydride (**2**, **Figure 2**). The metal hydride forms a metal-isopropoxide after the introduction of acetone (**3**, **Figure 2**) which exchanges with the alkoxy moiety to regenerate step (**1**) of the cycle.[13]

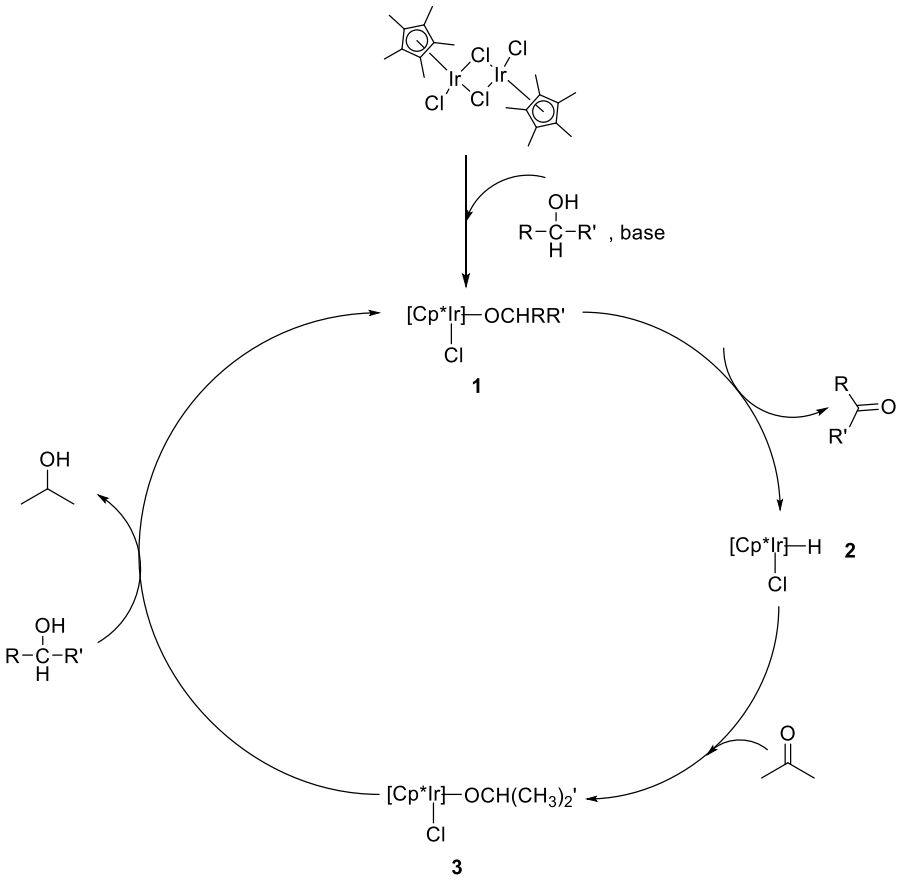

Figure 2. Mechanistic scheme for the oxidation of primary and secondary alcohols.

Fujita *et al*. expanded the catalytic use of $[Cp^*IrCl]_2(\mu^2\text{-}Cl)_2$ by using the dimeric complex for transfer hydrogenation of quinolines.[14] Tetrahydroquinoline derivatives are valuable synthetic intermediates that can be employed for pharmaceuticals, pesticides, and dyes.[15] Tetrahydroquinoline derivatives are normally produced using a metal catalyst in the presence of molecular hydrogen (H_2). Rather than using H_2 as a hydrogen source, Fujita showed a dimeric catalyst can act as a hydrogen transfer agent to produce 1,2,3,4-tetrahydroquinolines under mild conditions. The reaction of $[Cp^*IrCl]_2(\mu^2\text{-}Cl)_2$ with quinoline (**Figure 3**) produced 1,2,3,4-tetrahydroquinolines in 70% yield or better (**Table 3**).

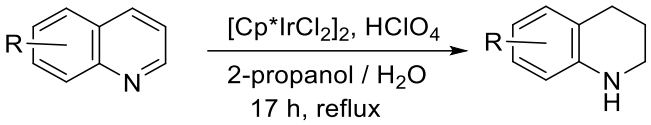

Figure 3. General schematic for the transfer hydrogenation of substituted quinolines.

Table 3. $[Cp^*IrCl]_2(\mu^2\text{-}Cl)_2$ catalyzed transfer hydrogenation of substituted quinolines.[a]

Entry	R	Cat. (mol%Ir)	$HClO_4$ (mol%)	Yield (%)[b]
1	H	1.0	10	(93)
2	H	2.0	0	89
3	2-Me	4.0	0	82
4	3-Me	2.0	10	79
5	4-Me	4.0	0	39
6	6-Me	2.0	10	78[c]
7	7-Me	2.0	10	78[c]
8	8-Me	2.0	10	82
9	5-NO_2	4.0	10	72
10	6-NO_2	2.0	10	94
11	6-Cl	2.0	10	78[c]
12	6-Br	2.0	10	70[c]
13	6-CO_2H	4.0	10	64
14	6-OMe	1.9	11	79[c]

[a] The reaction was carried out with quinolones (2.0 mmol), $[Cp^*IrCl]_2(\mu^2\text{-}Cl)_2$, and 60% $HClO_4$ (aq) in solvent (2-propanol 9.5 mL + H_2O 0.5 mL) under reflux for 17h. [b] Isolated yield. The value in parentheses was determined by GC. [c] Small amount of *N*-isopropyl-1,2,3,4-tetrahydroquinoline derivative was formed as byproduct (5-10%).[14]

Quinolines bearing a methyl group were reduced with yields of 78% or greater. However, the yield was decreased to 39% with the methyl in the 4 position. This phenomenon occurs due to competition between the methyl group and the catalyst for this position, resulting in a lower yield. Even with the addition of EWGs, the quinolines reacted with yields of 64% or better.

To begin the cycle (**Figure 4**), 2-propanol adds to generate the metal-isopropoxide (**1**). Next, β-hydride elimination of (**1**) forms the metal-hydride as seen in intermediate (**2**). The C=N of the quinolinium ion generated by the protonation of quinoline from $HClO_4$ inserts into the iridium-hydride bond to form 1,2-dihydroquinoline (**3a**). From there, the C=C bond of 1,2-

dihyrdoquinoline (**3a**) inserts into the iridium-hydride bond followed by protonolysis to give the hydroquinoline product (**4**).[14]

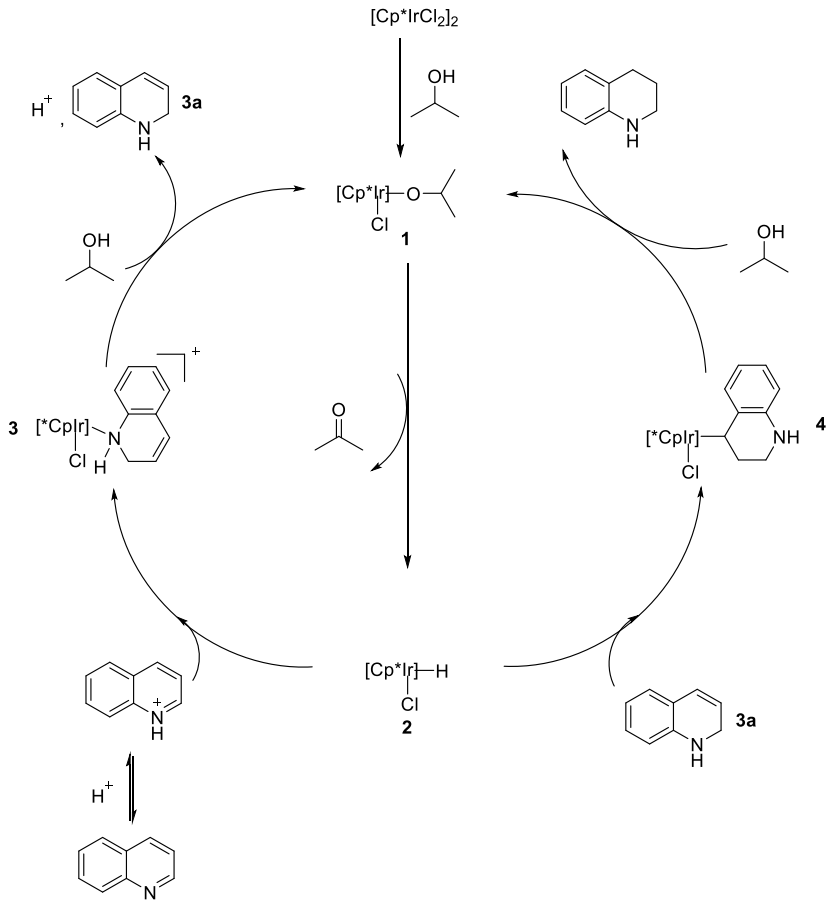

Figure 4. Mechanistic scheme for the transfer hydrogenation of quinolines catalyzed by $[Cp^*IrCl]_2(\mu^2\text{-}Cl)_2$.

Fujita *et al.* continued to work with group 9 metals and showed that $[Cp^*RhCl]_2(\mu^2\text{-}Cl)_2$ was an excellent catalyst for the synthesis of lactams from amino alcohols (**Figure 5**, schematic; **Table 4**, results; **Figure 6**, proposed mechanism). The yields improve from 80% to 96% or better with the addition of EWGs para to the amine (entries 2-4) suggesting that EWGs accelerate the reaction by making the amine more electrophilic. In the case of the cyano group (entry 5), the catalyst was deactivated due to its ability to coordinate to the metal.[16]

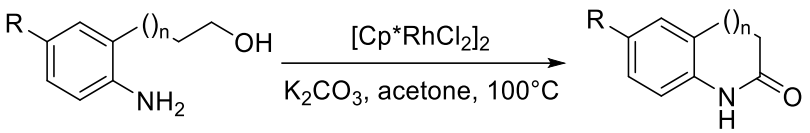

1a: n=1, R = H
1b: n=1, R = Cl
1c: n=1, R = CO_2Me
1d: n=1, R = COMe
1e: n=1, R = CN
1f: n=1, R = OMe
1g: n=1, R = Me
1h: n=2, R = H

2a: n=1, R = H
2b: n=1, R = Cl
2c: n=1, R = CO_2Me
2d: n=1, R = COMe
2e: n=1, R = CN
2f: n=1, R = OMe
2g: n=1, R = Me
2h: n=2, R = H

Figure 5. General schematic for the synthesis of various six-and seven-membered lactams from amino acids catalyzed by $[Cp^*RhCl]_2(\mu^2\text{-}Cl)_2$.

Table 4. Synthesis of various lactams from amino alcohols catalyzed by $[Cp^*RhCl]_2(\mu^2\text{-}Cl)_2$.[a]

Entry	Substrate	Product	Yield (%)[b]
1	**1a**	**2a**	80
2	**1b**	**2b**	96
3	**1c**	**2c**	97
4	**1d**	**2d**	96
5	**1e**	**2e**	71
6	**1f**	**2f**	63
7	**1g**	**2g**	96
8	**1h**	**2h**	86

[a] The reaction was carried out in a heavy-walled glass reactor at 100 °C for 20 h with amino alcohol (0.50 mmol), $[Cp^*RhCl]_2(\mu^2\text{-}Cl)_2$ (5.0% Rh), and K_2CO_3 (10%) in acetone (12.5 mL). [b] Isolated yield.[16]

The analogous rhodium dimeric species can act in two ways to form the corresponding lactams. To begin the cycle, the alcohol coordinates to the metal (**1**), followed by β-hydride elimination to produce an amino aldehyde (**2**) and form a metal-hydride (**3**). Acetone inserts to form the metal-isopropoxide (**4**), which exchanges with the amino alcohol to regenerate (**1**) in the catalytic cycle. Alternatively, the aldehyde may undergo condensation to form a cyclic hemiaminal (**5**). Oxidation of the hemiaminal by the catalyst proceeds via beta-hydrogen elimination to form the desired lactam (**6**).

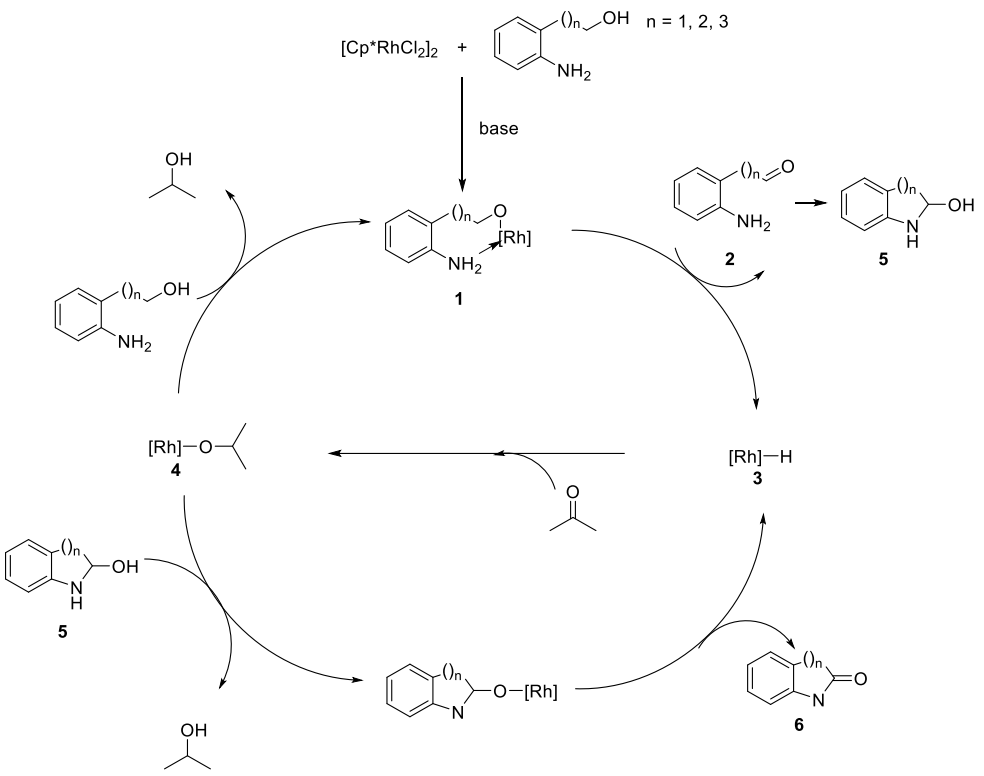

Figure 6. Mechanistic scheme for the synthesis of lactams catalyzed by $[Cp^*RhCl]_2(\mu^2\text{-}Cl)_2$.

1.2 Importance of half-sandwich complexes

Iridium and rhodium pentamethylcyclopentadienyl dimers have many catalytic applications; however, they are also used as synthetic precursors to half-sandwich complexes, also known as piano stool complexes, frequently by reaction with an excess of a bidentate ligand. The literature features an abundance of half-sandwich complexes with various chelating agents including amino alcohols,[17] amino acids,[6] ethylenediamines,[18] and C,N chelating ligands.[19] The facile synthesis of these compounds allows half-sandwich complexes to be easily tailored for catalytic and other applications.[3]

Suzuki *et al.* examined the use of $Cp^*IrCl[OCH_2C(C_6H_5)_2NH_2]$ for the oxidative lactonization of 1,4- or 1,5- diols (**Figure 7**) with greater than 95% yield, in most cases (**Table 5**).[20] Alkyl based diols and ring based diols were all successfully converted into their corresponding lactones. The less hindered hydroxyl group of unsymmetrical diols was oxidized to

produce the lactones in entries 9 and 10.[20] The proposed mechanism involves the oxidation of a hydroxyl to an aldehyde, which is in equilibrium with the lactol, followed by oxidation of the lactol to lactone (**Figure 8**).

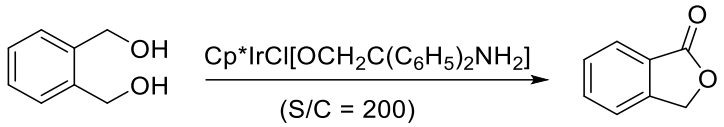

Figure 7. General schematic for the oxidative lactonization of diols catalyzed by $Cp^*IrCl[OCH_2C(C_6H_5)_2NH_2]$.

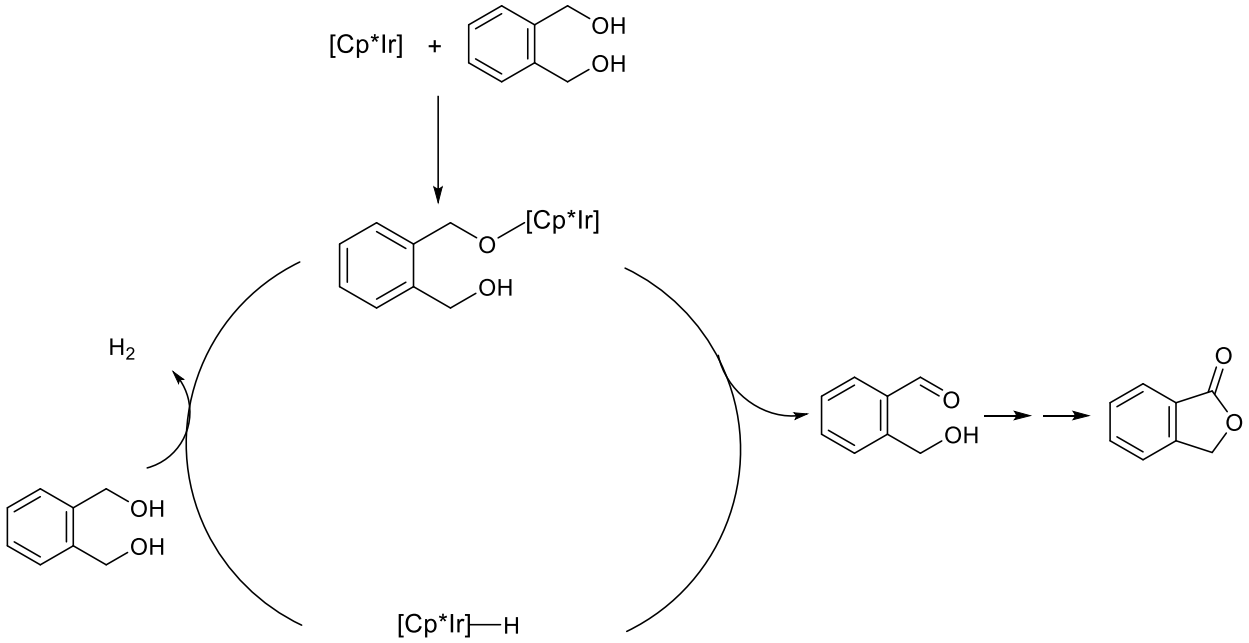

Figure 8. Mechanistic scheme for the synthesis of lactones catalyzed by $Cp^*IrCl[OCH_2C(C_6H_5)_2NH_2]$.

Table 5. Oxidative lactonization of diols catalyzed by an iridium catalyst.[a]

Entry	diol	time, h	product	% yield[b]
1	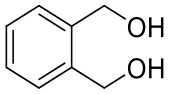	4	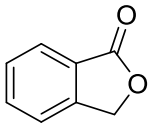	>99
2	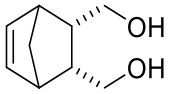	48	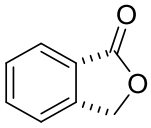	97
3	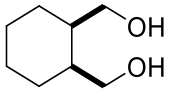	36	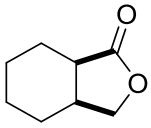	97
4	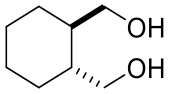	36	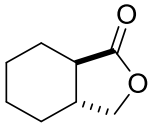	98
5	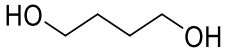	20	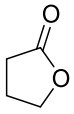	96
6[c]		48		89
7[d]	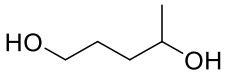	36	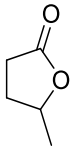	88
8[e]	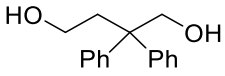	20	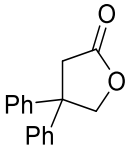	98
9	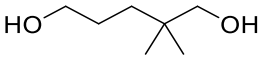	26	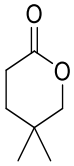	>99
10	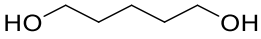	24	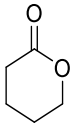	95
11[d]	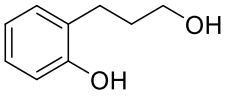	5	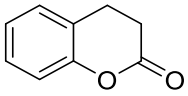	95

[a] Unless otherwise stated, the reaction was carried out at room temperature using a 1.0 M solution of diol (1.0 mmol) in acetone. Diol/Ir = 200:1. [b] Isolated yield. [c] Reaction using 50 g of 1e in 140 mL of 2-butanone (4.0 M) under reflux with a substrate/catalyst (S/C) ratio = 1000. [d] Reaction using a 2.0 M acetone solution. [e] The reaction was carried out using a 0.25 M solution of 1 g in CH_3CN containing 4 molar equiv. of acetone.

Morris *et al.* showed modified iridium amino acid complexes could be used as asymmetric transfer hydrogenation (ATH) catalysts for the reduction of ketones.[6] Morris demonstrated that the identity of the substituent on the Cp^{*R} ligand affected both conversion and enantiomeric excesses (ee's) in the reduction of pinacolone and acetophenone. The ee for the reduction of pinacolone was found to increase with a less rigid R ligand following the trend $Cp^{*phenyl} < Cp^{*benzyl} < Cp^{*isopropyl}$. The reduction of acetophenone followed the same trend seen in the reduction of pinacolone; however, these complexes generated low ee's. This result illustrates the value in exploring catalysts with modified Cp^{*R} ligands and their subsequent half-sandwich complexes.

Half-sandwich compounds have recently been used in chemotherapeutic and anti-microbial applications. Karpin *et al.* showed that iridium and rhodium amino acid complexes exhibited biological activity against various strains of mycobacteria, with minimum inhibitory concentrations (MIC) as low as 8 μg/mL.[18] Moreover, Sliwinska *et al*. examined the reaction of $[Cp^*MCl]_2(\mu^2\text{-}Cl)_2$ (M = Rh, Ir) with quinolin-8-ol, and the biological activity of the subsequent piano stool compound. Sliwinska showed that these piano stool compounds exhibit good activity as cytostatic and antibacterial agents as seen in **Table 6** and **Table 7**. Rhodium compounds were found to be more active against cancerous cells and bacteria than the corresponding iridium compounds.

Table 6. Antitumor activity of complexes **1** (Rh) and **2** (Ir).[21]

Tumor Cells	ID_{50} (μmol/L)	
	Complex **1**	Complex **2**
SK-Mel	0.8	0.8
SNB-19	5	9.8
C-32	0.9	4.9
SH-4	100	100

Table 7. Antibacterial activity of complexes **1** (Rh) and **2** (Ir).[21]

Microbe	MIC[a] (μg/mL)	
	Complex **1**	Complex **2**
E. coli	100	n.a.
K. pneumoniae	100	n.a.
P. aeruginosa	n.a.[b]	n.a.
M. luteus	3.12-6.25	25
S. aureus	3.12-6.25	25
E. faecalis	3.12-6.25	50
S. epiderimidis	<3.12	12.5

[a]MIC = minimum inhibitory concentration. [b] n.a. = nonactive.

Similarly, Sadler *et al.* examined the use of half-sandwich iridium complexes bearing N,N chelating moieties. Sadler showed that biological activity can be improved with increasing phenyl substituents with Cp^{*R} ligands, $Cp^{*phenyl}$ and $Cp^{*biphenyl}$. The increase in phenyl substituents enhanced lipophilicity and cell accumulation uptake, allowing the complexes to be comparable to cis-platin as anti-cancer agents for human ovarian cancer cells.[7a]

As indicated, rhodium and iridium pentasubstituted cyclopentadienyl dimeric complexes may be used in many catalytic or synthetic applications. Pentasubstituted cyclopentadienyl ligands of the type C_5Me_4R provide an opportunity to investigate the changes in catalytic activity and selectivity attributed to substituent variation.[6] The present work provides an effective way to synthesize these modified dimeric species in good yield using a microwave reactor.

1.3 Background of microwave-assisted synthesis

Microwave reactors have been shown to expedite the synthesis of organic and organometallic reactions, providing an alternative to time consuming conventional techniques.[22,23,24,25] In the electromagnetic spectrum, microwaves have wavelengths and frequencies between 0.001 - 1 m and 0.3 – 300 GHz, respectively.[26] A substance must possess a permanent dipole or have an induced dipole to generate heat when irradiated with microwaves.[26]

At the molecular level, a dipole is sensitive to an applied electric field as it will align itself with the electric field via rotation. As the frequency of the irradiation is low, the dipole can respond to the alternating electric field and therefore rotate. As a result, the continuous oscillating field generates a phase difference between the dipole and applied electric field. Consequently, the resulting energy is converted into heat as a result of the phase difference via molecular friction and collisions.[26-27] Heating in a closed vessel microwave reaction can rapidly reach higher temperatures due to the permittivity (ε), the ability to store charge, of a material. This allows an organic solvent to be heated beyond the conventional boiling point of the solvent, e.g. ethanol 79 °C vs 164 °C.[28]

Table 8 shows an important trend involving solvents with large permanent dipoles, i.e., ethanol, methanol, and water. Polar protic solvents are able to dissipate microwave energy more effectively than their nonpolar solvent counterparts, leading to more efficient localized heating than possible in a traditional benchtop reflux synthesis.[29] This results from the microwave energy introduced to the reactor not making contact with the vessel, allowing only the reacting chemicals and solvent to be heated.

Table 8. Value of relative permittivity (dielectric constant) at 20 °C for common solvents.[28]

Solvent	**Dielectric constant (ε_s)**
Benzene	2.3
Carbon tetrachloride	2.2
Chloroform	4.8
Acetone	21.4
Ethanol	25.7
Methanol	33.7
Water	80.4

The first use of a microwave reactor for organic synthesis was reported by Gedye *et al*. in 1986. Gedye's research showed reaction times were considerably shorter and yields were

comparable to or better than literature values in all cases.[30] In 1989, Baghurst *et al.* was the first to use a microwave reactor for organometallic synthesis. Baghurst's research demonstrated the synthesis of $[M(COD)]_2(\mu^2\text{-}Cl)_2$ (M = Rh, Ir) could be achieved with good yields in 1 minute or less.[22] Though it is well accepted that the microwave reactor provides a more efficient heating in syntheses and there are many examples of microwave chemistry,[29, 31] exactly how the "microwave effect" improves reaction time and yield is still highly debated.[32-32b, 33]

Many publications attribute the "microwave effect" to a purely thermal effect;[34] however, Moseley *et al.* dismisses this so-called effect, rationalizing instead that microwave radiation heats more uniformly than a traditional benchtop reflux.[27] In the current literature, microwave radiation cannot be solely explained via physical organic theory.[32b] Strauss emphasizes that kinetics of microwave reactors require more extensive experimentation in order to fully comprehend the benefits of microwave heating.[32a] As a result, the "microwave effect" remains ambiguous in the scientific community and the subject of much controversy.[32c, 33, 35]

1.4 Synthesis of iridium and rhodium dimers

Rhodium(III) and iridium(III) dimers $[Cp^*MCl]_2(\mu^2\text{-}Cl)_2$ (M = Rh, Ir) are conventionally obtained from refluxing $MCl_3 \cdot xH_2O$ and pentamethylcyclopentadiene in aqueous alcohol for 36-48 hours.[4, 31b] In addition to long reaction times, conventional syntheses of the $[Cp^{*R}MCl]_2(\mu^2\text{-}Cl)_2$ (M = Rh, Ir) cyclopentadiene derivatives yield less than 50% in some cases.[6-7] Improving yields of modified dimers is of great interest in order to effectively explore their application.

An alternative to the conventional synthesis of $[Cp^{*R}MCl]_2(\mu^2\text{-}Cl)_2$ (M = Rh, Ir) involves oxidation of the rhodium(I) and iridium(I) cyclooctadiene (COD) dimers with concentrated HCl. As COD is easily displaced with stronger coordinating ligands, dimeric cyclooctadiene compounds are excellent precursors to cyclopentadienyl dimers that are more challenging to synthesize.

Therefore, the reaction of $[M(COD)]_2(\mu^2\text{-}Cl)_2$ with the desired HCp^{*R} (**Figure 9**) will yield the corresponding pentasubstituted cyclopentadienyl dimeric complex.[36] Using this method, El Amouri *et al.* showed $[Cp^*IrCl]_2(\mu^2\text{-}Cl)_2$ can be synthesized in a 96% yield after benchtop reflux for 2.5 hours compared to the traditional 85% after a 48 hour reflux. Similarly, the synthesis of $[Cp^*RhCl]_2(\mu^2\text{-}Cl)_2$ was achieved in 91-93% yield.[36]

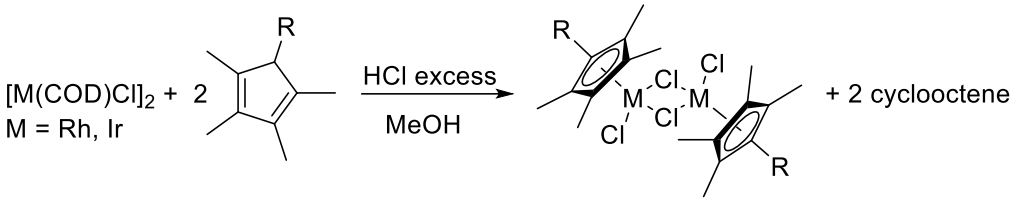

Figure 9. General scheme for the synthesis of $[Cp^{*R}MCl_2]_2(\mu^2\text{-}Cl)_2$ from $[M(COD)]_2(\mu^2\text{-}Cl)_2$ (M = Rh, Ir).

Yields and reaction times of pentamethylcyclopentadienyl dimers may be further improved by using a microwave reactor. Baghurst *et al*. showed that metal olefin dimers could be synthesized in $\leq$ 1 minute with similar or better yields than literature values.[29] However, reaction of $RhCl_3 \cdot xH_2O$ with some olefins, including cyclooctene and norbonylene, did not yield the dimer; rather, rhodium metal was the major product. This is because the reduction of the metal occurs faster than the coordination of the olefin to the rhodium.[22] Therefore, it is clear that microwave conditions need to be adjusted for the appropriate synthetic reaction.

1.5 Project design

The ability to alter the ancillary ligand, metal center, and chelating ligand of half-sandwich compounds allows for an extensive library of compounds to be examined. A modular approach to compound design allows various rhodium and iridium Cp* species to be tailored for catalytic or biological purposes. Rhodium and iridium were chosen as the metal center due to their known ability to act as transfer hydrogenation catalysts.

Pentasubstituted cyclopentadienyl ligands were chosen as they are more electron rich than their cyclopentadiene counterpart and are not easily displaced.[37] In addition, Cp*^{R} ligands block one face of the metal octahedron allowing for a facile modification of half-sandwich complexes. Alteration of the substituents on the pi ligand allows for examination of steric and electronic effects in many catalytic applications.[5, 37-38] Thus far, chain length has been shown to play an important role in inhibiting mycobacteria with amino acid half-sandwich complexes. Recently, Lucas *et al.* showed that Cp*^{R} terminal hydroxyl-functionalized iridium and rhodium dimers and complexes are not only efficient anti-cancer agents, but the length of the chain on the Cp*^{R} affects activity.[39] Furthermore, Deng *et al.* have shown that increasing chain length of catalysts leads to a stabilizing interaction with long chain substrates.[40]

Transfer hydrogenation involving pentasubstituted cyclopentadienyl rhodium and iridium dimers has rarely been explored. Moreover, the few dimers that have previously been reported, were synthesized in poor yield. The time, reagents, purification techniques, and loss of expensive metal required to yield modified pentasubstituted cyclopentadienyl dimers are quite expensive. The work reported henceforth describes the successful use of a microwave reactor to synthesize iridium and rhodium dimeric cyclopentadienyl complexes with yields ranging from 15.5 - 95.7%. This alternate approach was developed based on modifications to previously reported methodology in order to provide an efficient and cost effective pathway to further iridium and rhodium dimers.

Chapter 2 Experimental

2.1 Materials and Instruments

2.1.1 Materials and Methods

All materials for synthesis, purification, and characterization were used as received unless otherwise stated. Snap ring tops and 10 mL pressure tubes were purchased from CEM Corporation. $RhCl_3 \cdot xH_2O$ and $IrCl_3 \cdot xH_2O$ were purchased from Pressure Chemical, Pittsburgh, PA 15201. Heptylmagnesium chloride, and 2,3,4,5-tetramethylcyclopent-2-en-1-one were purchased from Alfa Aesar, Ward Hill, MA 01835. Reagent grade solvents, ethyl-tetramethylcyclopentadiene, tetramethyl(*n*-propyl)cyclopentadiene, benzylmagnesium chloride, cyclohexylmagnesium chloride, cyclopentylmagnesium bromide, phenylmagnesium bromide, phenethylmagnesium chloride, isopropylmagnesium bromide, butylmagnesium chloride, isobutylmagnesium chloride, *sec*-butylmagnesium chloride, pentylmagnesium bromide, hexylmagnesium bromide, and octylmagnesium bromide were purchased from Sigma Aldrich, St. Louis, MO 63103. Deuterated solvents for NMR spectroscopy were obtained from Cambridge Isotope Laboratories. Elemental analyses were performed by Atlantic Microlabs, Norcross, GA. ^{1}H NMR and ^{13}C NMR spectra were collected on a Varian MR-400 NMR spectrometer. ^{13}C NMR spectra were correspondingly recorded at 101 MHz. The following abbreviations are used to show coupling in the spectra: s (singlet), d (doublet), t (triplet), q (quartet), quin (quintet), sep (septet), m (multiplet), dd (doublet of doublets), tt (triplet of triplets), and qt (quartet of triplets).

2.1.2 High Resolution Mass Spectrometry

Mass spectrometry was performed by William Bebout of the Virginia Tech Chemistry Department Analytical Service laboratory in Blacksburg, VA. Positive ion electrospray ionization mass spectra ((+)ESI-MS)122 were collected using an Agilent Technologies 6220 Accurate-Mass time-of-flight

(TOF) LC-MS with a dual ESI source. The sample was dissolved in HPLC grade solvent and injected through a preloading capillary at 1.2 kV with a flow rate of 0.4 mL/min. N_2 gas was used as the inert nebulizing gas at a pressure of 60 psig. The charging voltage was set to 2000 V, the fragmentor voltage set to 125 V, and the skimmer voltage set to 65 V.

2.1.3 Single X-ray Crystal Collection and Data Analysis:

X-ray crystallographic data was collected at 100 K on an Oxford Diffraction Gemini diffractometer with an EOS CCD detector and Mo Kα radiation. Crystals were coated in Paratone® oil and mounted on a fiber loop. Data collection and data reduction were performed using Agilent's CrysAlis Pro software. Structure solution and refinement were performed with ShelXS and ShelXL, and Olex2 was used for graphical representation of the data.

2.2 Synthesis

2.2.1 General procedure for synthesis of $[Cp^{*R}RhCl]_2(\mu^2\text{-}Cl)_2$

A microwave pressure tube was fitted with the appropriate amounts of the respective $[Rh(COD)]_2(\mu^2\text{-}Cl)_2$, HCp^{*R}, in 4 mL of methanol with 0.5 mL of concentrated HCl. The reaction mixture was heated to 115 °C at 50 watts and 150 psi and held for 1 hour, yielding a red solution. The solvent was evaporated under reduced pressure, and the resulting powder recrystallized from DCM and cold hexanes, collected via filtration, and washed with cold hexanes.

2.2.1.1 Synthesis of $[Cp^{*ethyl}RhCl]_2(\mu^2\text{-}Cl)_2$ (**1a**)

Following the general procedure, $[Rh(COD)]_2(\mu^2\text{-}Cl)_2$ (0.250 g, 0.507 mmol), Cp^{*ethyl} (0.244 g, 1.62 mmol), and 0.5 mL of HCl were reacted in methanol (4 mL) to give **1a** (0.259 g, 79.0% yield). ^{1}H NMR (400 MHz, $CDCl_3$) δ 2.27 – 2.23 (q, 4H), 1.61 (s, 12 H), 1.60 (s, 12H), 1.01-0.97 (t, 6 H). ^{13}C NMR (101 MHz, $CDCl_3$) δ 97.41-97.31 (d, *J* = 9.3 Hz), 94.76-94.66 (d, *J* = 9.2 Hz), 94.00-93.91 (d, *J* = 9.1 Hz), 17.61, 11.55, 9.51, 9.30.

HRMS/ESI+ (m/z): Calc. for $C_{22}H_{34}Cl_3Rh_2$ 608.9836; Found 608.9761

2.2.1.2 Synthesis of $[Cp^{*n\text{-propyl}}RhCl]_2(\mu^2\text{-}Cl)_2$ **1b**

Following the general procedure, $[Rh(COD)]_2(\mu^2\text{-}Cl)_2$ (0.150 g, 0.304 mmol) of, $Cp^{*n\text{-propyl}}$ (0.200 g, 1.22 mmol), and 0.5 mL of HCl were reacted in methanol (4 mL) to give **1b** (0.164 g, 80.0% yield). ^{1}H NMR (400 MHz, $CDCl_3$) δ 2.27 – 2.23 (t, 4H), 1.64 (s, 12 H), 1.62 (s, 12H), 1.45-1.36 (m, 4H), 0.94-0.91 (t, 6 H). ^{13}C NMR (101 MHz, $CDCl_3$) δ 96.17-96.07 (d, *J* = 9.4 Hz), 94.71-94.62 (d, *J* = 9.2 Hz), 94.34-94.25 (d, *J* = 9.3 Hz), 26.04, 20.89, 14.31, 9.59, 9.53.

HRMS/ESI+ (m/z): Calc. for $C_{24}H_{38}Cl_3Rh_2$ 637.0149; Found 637.0173

Anal. Calc. for $C_{24}H_{38}Cl_4Rh_2$, C, 42.76; H, 5.68; Found, C, 42.47; H, 5.68

2.2.1.3 Synthesis of $[Cp^{*isopropyl}RhCl]_2(\mu^2\text{-}Cl)_2$ **1c**

Following the general procedure, $[Rh(COD)]_2(\mu^2\text{-}Cl)_2$ (0.200 g, 0.406 mmol), $Cp^{*isopropyl}$ (0.267 g, 1.62 mmol), and 0.5 mL of HCl were reacted in methanol (4 mL) to give **1c** (0.042 g, 15.5% yield) . ^{1}H NMR (400 MHz, $CDCl_3$) δ 2.66 – 2.55 (sept, 2H), 1.72 (s, 12 H), 1.60 (s, 12H), 1.31-1.29 (d, 12H). ^{13}C NMR (101 MHz, $CDCl_3$) δ 97.71-97.62 (d, *J* = 9.1 Hz), 95.44-95.34 (d, *J* = 10.0 Hz), 94.22-94.13 (d, *J* = 9.2 Hz), 25.09, 20.79, 10.51, 9.62.

HRMS/ESI+ (m/z): Calc. for $C_{24}H_{38}Cl_3Rh_2$ 637.0149; Found 637.014

2.2.1.4 Synthesis of $[Cp^{*n\text{-butyl}}RhCl]_2(\mu^2\text{-}Cl)_2$ **1d**

Following the general procedure, $[Rh(COD)]_2(\mu^2\text{-}Cl)_2$ (0.200 g, 0.406 mmol), $Cp^{*n\text{-butyl}}$ (0.289 g, 1.62 mmol), and 0.5 mL of concentrated HCl were reacted in methanol (4 mL) to give **1d** (0.180 g, 63.1%). ^{1}H NMR (400 MHz, $CDCl_3$) δ 2.27 – 2.24 (t, 4H), 1.63 (s, 12 H), 1.61 (s, 12H), 1.38-1.27 (m, 8H), 0.90-0.87 (t, 6 H). ^{13}C NMR (101 MHz, $CDCl_3$) δ 96.33-96.24 (d, *J* = 9.6 Hz), 94.64-94.55 (d, *J* = 9.2 Hz), 94.26-94.17 (d, *J* = 9.2 Hz), 29.76, 23.85, 22.90, 13.96, 9.54, 9.53.

HRMS/ESI+ (m/z): Calc. for $C_{26}H_{42}Cl_3Rh_2$ 665.0462; Found 665.0447

Anal. Calc. for $C_{26}H_{42}Cl_4Rh_2$, C, 44.47; H, 6.03; Found, C, 44.55; H, 5.96

2.2.1.5 Synthesis of $[Cp^{*isobutyl}RhCl]_2(\mu^2\text{-}Cl)_2$ **1e**

Following the general procedure, $[Rh(COD)]_2(\mu^2\text{-}Cl)_2$ (0.200 g, 0.406 mmol), $Cp^{*isobutyl}$ (0.362 g, 2.03 mmol), and 0.5 mL of HCl were reacted in methanol (4 mL) to give **1e** (0.252 g, 88.5% yield). ^{1}H NMR (400 MHz, $CDCl_3$) δ 2.19 – 2.17 (d, 4H), 1.73-1.64 (m, 2H), 1.63 (s, 12 H), 1.62 (s, 12H), 0.88-0.87 (d, 12 H). ^{13}C NMR (101 MHz, $CDCl_3$) δ 95.58-95.49 (d, *J* = 9.4 Hz), 94.74-94.66 (d, *J* = 9.2 Hz), 94.70-94.61 (d, *J* = 9.2 Hz), 32.93, 27.98, 23.84, 10.09, 9.58.

HRMS/ESI+ (m/z): $C_{26}H_{42}Cl_3Rh_2$ 665.0462; Found 665.0459

Anal. Calc. for $C_{26}H_{42}Cl_4Rh_2$, C, 44.47; H, 6.03; Found, C, 44.18; H, 5.96

2.2.1.6 Synthesis of $[Cp^{*sec\text{-}butyl}RhCl]_2(\mu^2\text{-}Cl)_2$ **1f**

Following the general procedure, $[Rh(COD)]_2(\mu^2\text{-}Cl)_2$, $Cp^{*sec\text{-}butyl}$ (0.289 g, 1.62 mmol), and 0.5 mL of HCl were reacted in methanol (4 mL). Upon cooling, an orange-yellow powder (0.123 g) formed in a red solution. The powder was isolated and the red solution evaporated under reduced pressure. The resulting red powder was recrystallized from DCM and cold hexanes and collected by filtration. The red powder was washed with cold hexanes to give **1f** in a reacted yield of 0.0589 g (54.0%). ^{1}H NMR (400 MHz, $CDCl_3$) δ 2.37 – 2.28 (m, 2H), 1.72 (s, 6H), 1.69 (s, 6H), 1.67 – 1.64 (m, 2 H), 1.61 (s, 6H), 1.60 (s, 6H), 1.51 – 1.42 (m, 2 H), 1.39 – 1.37 (d, 6 H), 0.90 – 0.86 (t, 6 H). ^{13}C NMR (101 MHz, $CDCl_3$) δ 98.37-98.29 (d, *J* = 8.8 Hz), 97.61-97.53 (d, *J* = 8.9 Hz), 95.35-95.25 (d, *J* = 10.1 Hz), 95.29-95.20 (d, *J* = 9.0 Hz), 92.83-92.73 (d, *J* = 9.4 Hz), 31.65, 27.79, 18.41, 12.65, 10.89, 10.45, 9.83, 9.44.

HRMS/ESI+ (m/z): $C_{26}H_{42}Cl_3Rh_2$ 665.0462; Found 665.0472

2.2.1.7 Synthesis of $[Cp^{*n\text{-pentyl}}RhCl]_2(\mu^2\text{-}Cl)_2$ **1g**

Following the general procedure, $[Rh(COD)]_2(\mu^2\text{-}Cl)_2$ (0.200 g, 0.406 mmol), $Cp^{*n\text{-pentyl}}$ (0.312 g, 1.62 mmol), and 0.5 mL of HCl were reacted in methanol (4 mL) to give **1g (**0.227 g, 76.5%). ^{1}H NMR (400 MHz, $CDCl_3$) δ 2.27 – 2.23 (t, 4H), 1.63 (s, 12 H), 1.62 (s, 12H), 1.38-1.24 (m, 12H), 0.87-0.84 (t, 6 H). ^{13}C NMR (101 MHz, $CDCl_3$) δ 96.27-96.18 (d, *J* = 9.3 Hz), 94.53-94.44 (d, *J* = 9.1 Hz), 94.12-94.03 (d, *J* = 9.2 Hz), 31.71, 27.16, 23.93, 13.80, 9.41, 9.39.

HRMS/ESI+ (m/z): Calc. for $C_{28}H_{46}Cl_3Rh_2$ 693.0775; Found 693.0788

Anal. Calc. for $C_{28}H_{46}Cl_4Rh_2$, C, 46.05; H, 6.35; Found, C, 45.77; H, 6.16

2.2.1.8 Synthesis of $[Cp^{*n\text{-hexyl}}RhCl]_2(\mu^2\text{-}Cl)_2$ **1h**

Following the general procedure, $[Rh(COD)]_2(\mu^2\text{-}Cl)_2$ (0.200 g, 0.304 mmol), $Cp^{*n\text{-hexyl}}$ (0.344 g, 1.62 mmol), and 0.5 mL of HCl were reacted in methanol (4 mL) to give **1h** (0.224 g, 72.7% yield). ^{1}H NMR (400 MHz, $CDCl_3$) δ 2.26 – 2.23 (t, 4H), 1.63 (s, 12 H), 1.61 (s, 12H), 1.37-1.24 (m, 14H), 0.87-0.84 (t, 6 H).^{13}C NMR (101 MHz, $CDCl_3$) δ 96.41-96.31 (d, *J* = 9.4 Hz), 94.68-94.59 (d, *J* = 9.1 Hz), 94.26-94.17 (d, *J* = 9.3 Hz), 31.61, 29.46, 27.62, 24.14, 22.58, 14.13, 9.57, 9.55.

HRMS/ESI+ (m/z): Calc. for $C_{30}H_{50}Cl_3Rh_2$ 721.1088; Found 721.1106

2.2.1.9 Synthesis of $[Cp^{*n\text{-heptyl}}RhCl]_2(\mu^2\text{-}Cl)_2$ **1i**

Following the general procedure, $[Rh(COD)]_2(\mu^2\text{-}Cl)_2$ (0.150 g, 0.304 mmol), $Cp^{*n\text{-heptyl}}$ (0.344 g, 1.62 mmol), and 0.5 mL of HCl were reacted in methanol (4 mL) to give **1i** (0.125g, 52.2% yield). ^{1}H NMR (400 MHz, $CDCl_3$) δ 2.26 – 2.22 (t, 4H), 1.63 (s, 12 H), 1.61 (s, 12H), 1.33-1.22 (m, 20H), 0.87-0.83 (t, 6 H).^{13}C NMR (101 MHz, $CDCl_3$) δ 96.41-96.32 (d, *J* = 9.5 Hz), 94.69-94.60 (d, *J* = 9.2 Hz), 94.26-94.17 (d, *J* = 9.2 Hz), 31.77, 29.76, 29.13, 27.66, 24.13, 22.17, 14.20, 9.57, 9.55.

HRMS/ESI+ (m/z): Calc. for $C_{32}H_{54}Cl_3Rh_2$ 749.1401; Found 749.1413

Anal. Calc. for $C_{32}H_{54}Cl_4Rh_2$, C, 48.88; H, 6.92; Found, C, 49.11; H, 6.87

2.2.1.10 Synthesis of $[Cp^{*n\text{-octyl}}RhCl]_2(\mu^2\text{-}Cl)_2$ **1j**

Following the general procedure, $[Rh(COD)]_2(\mu^2\text{-}Cl)_2$ (0.200 g, 0.304 mmol), $Cp^{*n\text{-octyl}}$ (0.344 g, 1.62 mmol), and 0.5 mL of HCl were reacted in methanol (4 mL) to give **1j** (0.173 g, 52.3% yield). ^{1}H NMR (400 MHz, $CDCl_3$) δ 2.26 – 2.22 (t, 4H), 1.63 (s, 12 H), 1.61 (s, 12H), 1.29-1.23 (m, 24H), 0.87-0.84 (t, 6 H).^{13}C NMR (101 MHz, $CDCl_3$) δ 96.41-96.32 (d, *J* = 9.5 Hz), 94.69-94.60 (d, *J* = 9.2 Hz), 94.26-94.17 (d, *J* = 9.2 Hz), 32.23, 30.12, 29.74, 29.53, 27.98, 24.46, 23.07, 14.53, 9.89, 9.87.

HRMS/ESI+ (m/z): Calc. for $C_{34}H_{58}Cl_3Rh_2$ 777.1717; Found 777.1701

Anal. Calc. for $C_{34}H_{58}Cl_4Rh_2$, C, 50.14; H, 7.18; Found, C, 50.43; H, 7.09

2.2.1.11 Synthesis of $[Cp^{*phenyl}RhCl]_2(\mu^2\text{-}Cl)_2$ **1k**

Following the general procedure, $[Rh(COD)]_2(\mu^2\text{-}Cl)_2$ (0.200 g, 0.406 mmol), $Cp^{*phenyl}$ (0.322 g, 1.62 mmol), and 0.5 mL of HCl were reacted in methanol (4 mL) to give **1k** (0.225 g, 74.6%). ^{1}H NMR (400 MHz, $CDCl_3$) δ 7.66 – 7.64 (m, 4H), 7.39 – 7.36 (m, 6H), 7.08-7.06 (m, 4 H), 1.71 (s, 12 H), 1.68 (s, 12H). ^{13}C NMR (101 MHz, $CDCl_3$) δ 130.36, 129.02, 128.74, 128.41, 100.47-100.39 (d, *J* = 8.6 Hz), 93.67-93.58 (d, *J* = 9.0 Hz), 90.70-90.60 (d, *J* = 10.2 Hz), 10.75, 9.75.

HRMS/ESI+ (m/z): Calc. for $C_{30}H_{34}Cl_3Rh_2$ 704.9836; Found 704.9854

*Previously reported[41]

2.2.1.12 Synthesis of $[Cp^{*benzyl}RhCl]_2(\mu^2\text{-}Cl)_2$ **1l**

Following the general procedure, $[Rh(COD)]_2(\mu^2\text{-}Cl)_2$ (0.200 g, 0.406 mmol), $Cp^{*benzyl}$ (0.344 g, 1.62 mmol), and 0.5 mL of HCl were reacted in methanol (4 mL) to give **1l** (0.276 g, 88.5% yield). ^{1}H NMR (400 MHz, $CDCl_3$) δ 7.28 – 7.25 (m, 2H), 7.24 – 7.18 (m, 4H), 7.08-7.06 (m, 4 H), 3.71 (s, 4 H), 1.67 (s, 12 H), 1.65 (s, 12H). ^{13}C NMR (101 MHz, $CDCl_3$) δ 136.17, 128.81, 128.26,

126.86, 95.09-95.00 (d, *J* = 9.1 Hz), 94.94-94.85 (d, *J* = 9.0 Hz), 93.98-93.88 (d, *J* = 9.5 Hz), 30.14, 9.87, 9.44.

HRMS/ESI+ (m/z): Calc. for $C_{32}H_{38}Cl_3Rh_2$ 733.0149; Found 733.0158

Anal. Calc. for $C_{32}H_{38}Cl_4Rh_2$, C, 49.90; H, 4.97; Found, C, 50.49; H, 5.19

2.2.1.13 Synthesis of $[Cp^{*phenethyl}RhCl]_2(\mu^2\text{-}Cl)_2$ **1m**

Following the general procedure, $[Rh(COD)]_2(\mu^2\text{-}Cl)_2$ (0.150 g, 0.304 mmol), $Cp^{*phenethyl}$ (0.274 g, 1.22 mmol), and 0.5 mL of HCl were reacted in methanol (4 mL) to give **1m** (0.186 g, 76.7% yield). ^{1}H NMR (400 MHz, $CDCl_3$) δ 7.23 – 7.14 (m, 6H), 6.99 – 6.97 (dd, 4H), 2.72-2.69 (t, 4 H), 2.61-2.57 (t, 4 H), 1.57 (s, 12 H), 1.36 (s, 12H). ^{13}C NMR (101 MHz, $CDCl_3$) δ 139.75, 128.60, 128.50, 126.47, 94.82-94.73 (d, *J* = 9.1 Hz), 94.61-94.52 (d, *J* = 9.5 Hz), 94.44-94.35 (d, *J* = 9.2 Hz), 33.37, 26.45, 14.26, 9.32, 9.12.

HRMS/ESI+ (m/z): Calc. for $C_{34}H_{38}Cl_3Rh_2$ 761.0462; Found 761.0466

Anal. Calc. for $C_{34}H_{38}Cl_4Rh_2$, C, 51.15; H, 5.30; Found, C, 50.89; H, 5.18

2.2.1.14 Synthesis of $[Cp^{*cyclohexyl}RhCl]_2(\mu^2\text{-}Cl)_2$ **1n**

Following the general procedure, $[Rh(COD)]_2(\mu^2\text{-}Cl)_2$ (0.200 g, 0.406 mmol), $Cp^{*cyclohexyl}$ (0.332 g, 1.62 mmol), and 0.5 mL of HCl were reacted in methanol (4 mL). Upon cooling, an orange-yellow powder (0.091 g) formed in a red solution. The powder was isolated and the red solution evaporated under reduced pressure. The resulting red powder was recrystallized from DCM and cold hexanes and collected by filtration. The red powder was washed with cold hexanes to give **1n** in a reacted yield of 0.106 g (63.6%). ^{1}H NMR (400 MHz, $CDCl_3$) δ 2.20 – 2.12 (tt, 2H), 2.01 – 1.98 (m, 4H), 1.79 – 1.75 (m, 4H), 1. 71 (s, 12 H), 1.69 (s, 12H), 1.44 – 1.25 (m, 10H), 1.19 – 1.08 (qt, 2H). ^{13}C NMR (101 MHz, $CDCl_3$) δ 97.80-97.71 (d, *J* = 8.9 Hz), 93.92-93.83 (d, *J* = 9.1 Hz), 93.68-93.59 (d, *J* = 9.1 Hz), 35.24, 30.60, 26.67, 25.97, 10.63, 9.51.

HRMS/ESI+ (m/z): Calc. for $C_{30}H_{46}Cl_3Rh_2$ 717.0775; Found 717.0782

Anal. Calc. for $C_{30}H_{46}Cl_4Rh_2$, C, 47.77; H, 6.15; Found, C, 47.27; H, 5.88

2.2.1.15 Synthesis of $[Cp^{*cyclopentyl}RhCl]_2(\mu^2\text{-}Cl)_2$ **1o**

Following the general procedure, $[Rh(COD)]_2(\mu^2\text{-}Cl)_2$ (0.150 g, 0.304 mmol), $Cp^{*cyclopentyl}$ (0.232 g, 1.22 mmol), and 0.5 mL of HCl were reacted in methanol (4 mL). Upon cooling, an orange-yellow powder (0.031 g) formed in a red solution. The powder was isolated and the red solution evaporated under reduced pressure. The resulting red powder was recrystallized from DCM and cold hexanes and collected by filtration. The red powder was washed with cold hexanes to give **1o** in a reacted yield of 0.095 g (53.9%).^{1}H NMR (400 MHz, $CDCl_3$) δ 2.71 – 2.62 (quin, 2H), 2.13 – 2.06 (m, 4H), 1. 72 (s, 12 H), 1.69 – 1.62 (m, 12H), 1.60 (s, 12H). ^{13}C NMR (101 MHz, $CDCl_3$) δ 97.15-97.05 (d, *J* = 9. 0 Hz), 94.56-94.47 (d, *J* = 9.0 Hz), 93.97-93.88 (d, *J* = 9.3 Hz), 35.63, 31.60, 26.69, 10.56, 9.68.

HRMS/ESI+ (m/z): Calc. for $C_{28}H_{42}Cl_3Rh_2$ 689.0462; Found 689.0503

2.2.2 General procedure for synthesis of $[Cp^{*R}IrCl]_2(\mu^2\text{-}Cl)_2$

A microwave pressure tube was fitted with the appropriate amounts of the respective $[Ir(COD)]_2(\mu^2\text{-}Cl)_2$, HCp^{*R}, in 4 mL of methanol with 0.5 mL of concentrated HCl. The reaction mixture was heated to 115 °C at 50 watts and 150 psi and held for 1 hour, yielding an orange solution. The solvent was evaporated under reduced pressure and the resulting powder recrystallized from DCM and cold hexanes, collected via filtration, and washed with cold hexanes.

2.2.2.1 Synthesis of $[Cp^{*ethyl}IrCl]_2(\mu^2\text{-}Cl)_2$ **2a**

Following the general procedure, $[Ir(COD)]_2(\mu^2\text{-}Cl)_2$ (0.100 g, 0.149 mmol), Cp^{*ethyl} (0.045 g, 0.298 mmol), and 0.5 mL of HCl were reacted in methanol (4 mL) to give **2a** (0.061 g, 50.0%

yield). ^{1}H NMR (400 MHz, $CDCl_3$) δ 2.16 – 2.10 (q, 4H), 1.58 (s, 12 H), 1.56 (s, 12H), 1.07-1.03 (t, 6 H). ^{13}C NMR (101 MHz, $CDCl_3$) δ 89.06, 86.49, 86.18, 17.56, 11.63, 9.30, 9.13.

Anal. Calc. for $C_{22}H_{34}Cl_4Ir_2$, C, 32.04; H, 4.16; Found, C, 31.88; H, 3.96

2.2.2.2 Synthesis of $[Cp^{*n\text{-propyl}}IrCl]_2(\mu^2\text{-}Cl)_2$ **2b**

Following the general procedure, $[Ir(COD)]_2(\mu^2\text{-}Cl)_2$ (0.100 g, 0.149 mmol), $Cp^{*n\text{-propyl}}$ (0.0851 g, 0.521 mmol), and 0.5 mL of HCl were reacted in methanol (4 mL) to give **2b** (0.078 g, 61.4% yield). ^{1}H NMR (400 MHz, $CDCl_3$) δ 2.14 – 2.10 (q, 4H), 1.61 (s, 12 H), 1.59 (s, 12H), 1.49-1.40 (m, 4H), 0.95-0.91 (t, 6 H). ^{13}C NMR (101 MHz, $CDCl_3$) δ 87.86, 86.42, 86.41, 26.05, 20.89, 14.26, 9.46, 9.37.

HRMS/ESI+ (m/z): $C_{24}H_{38}[^{193}Ir]_2Cl_3$ 817.1298; Found 817.1331

2.2.2.3 Synthesis of $[Cp^{*isopropyl}IrCl]_2(\mu^2\text{-}Cl)_2$ **2c**

Following the general procedure, $[Ir(COD)]_2(\mu^2\text{-}Cl)_2$ (0.100 g, 0.149 mmol), $Cp^{*isopropyl}$ (0.0851 g, 0.521 mmol), and 0.5 mL of HCl were reacted in methanol (4 mL) to give **2c** (0.089 g, 69.9% yield). ^{1}H NMR (400 MHz, $CDCl_3$) δ 2.54 – 2.43 (sept, 2H), 1.68 (s, 12 H), 1.60 (s, 12H), 1.29-1.27 (d, 12 H). ^{13}C NMR (101 MHz, $CDCl_3$) δ 90.38, 86.47, 86.21, 25.39, 20.78, 10.40, 9.88.

HRMS/ESI+ (m/z): $C_{24}H_{38}[^{193}Ir]_2Cl_3$ 817.1298; Found 817.1326

Anal. Calc. for $C_{24}H_{38}Cl_4Ir_2$, C, 33.80; H, 4.49; Found, C, 34.01; H, 4.48

2.2.2.4 Synthesis of $[Cp^{*n\text{-butyl}}IrCl]_2(\mu^2\text{-}Cl)_2$ **2d**

Following the general procedure, $[Ir(COD)]_2(\mu^2\text{-}Cl)_2$ (0.300 g, 0.447 mmol), $Cp^{*n\text{-butyl}}$ (0.159 g, 0.893 mmol), and 0.5 mL of HCl were reacted in methanol (4 mL) to give **2d** (0.109 g, 55.3% yield). ^{1}H NMR (400 MHz, $CDCl_3$) δ 2.15 – 2.11 (t, 4H), 1.60 (s, 12 H), 1.58 (s, 12H), 1.41-1.28 (m, 4H), 0.91-0.88 (t, 6 H). ^{13}C NMR (101 MHz, $CDCl_3$) δ 88.09, 86.41, 86.39, 29.80, 23.88, 22.83, 13.87, 9.38, 9.34.

HRMS/ESI+ (m/z): $C_{26}H_{42}[^{193}Ir]_2Cl_3$ 845.1611; Found 845.1617

Anal. Calc. for $C_{26}H_{42}Cl_4Ir_2$, C, 35.45; H, 4.81; Found, C, 35.61; H, 4.80

2.2.2.5 Synthesis of $[Cp^{*isobutyl}IrCl]_2(\mu^2\text{-}Cl)_2$ **2e**

Following the general procedure, $[Ir(COD)]_2(\mu^2\text{-}Cl)_2$ (0.200 g, 0.298 mmol), $Cp^{*isobutyl}$ (0.186 g, 1.04 mmol), and 0.5 mL of HCl were reacted in methanol (4 mL) to give **2e** (0.199 g, 75.7% yield). ^{1}H NMR (400 MHz, $CDCl_3$) δ 2.06 – 2.04 (d, 4H), 1.77-1.66 (m, 2H), 1.61 (s, 12 H), 1.60 (s, 12H), 0.90-0.89 (d, 12 H). ^{13}C NMR (101 MHz, $CDCl_3$) δ 87.32, 86.83, 86.42, 32.96, 27.75, 22.67, 9.92, 9.38.

HRMS/ESI+ (m/z): $C_{26}H_{42}[^{193}Ir]_2Cl_3$ 845.1611; Found 845.1602

Anal. Calc. for $C_{26}H_{42}Cl_4Ir_2$, C, 35.45; H, 4.81; Found, C, 35.66; H, 4.70

2.2.2.6 Synthesis of $[Cp^{*sec\text{-}butyl}IrCl]_2(\mu^2\text{-}Cl)_2$ **2f**

Following the general procedure, $[Ir(COD)]_2(\mu^2\text{-}Cl)_2$ (0.500 g, 0.744 mmol), $Cp^{*sec\text{-}butyl}$ (0.465 g, 2.61 mmol), and 0.5 mL of HCl were reacted in methanol (4 mL) to give **2f** (0.6276 g, 95.7% yield). ^{1}H NMR (400 MHz, $CDCl_3$) δ 2.23 – 2.18 (m, 2H), 1.68 (s, 6H), 1.66 – 1.67 (m, 2 H), 1.66 (s, 6H), 1.62 (s, 6H), 1.58 (s, 6H), 1.53 – 1.43 (m, 2 H), 1.33 – 1.31 (d, 6 H), 0.90 – 0.86 (t, 6 H). ^{13}C NMR (101 MHz, $CDCl_3$) δ 91.03, 90.44, 87.08, 86.29, 85.01, 32.04, 27.71, 18.47, 12.84, 10.77, 10.40, 9.82, 9.61.

HRMS/ESI+ (m/z): $C_{26}H_{42}[^{193}Ir]_2Cl_3$ 845.1611; Found 845.1695

Anal. Calc. for $C_{26}H_{42}Cl_4Ir_2$, C, 35.45; H, 4.81; Found, C, 35.19; H, 4.71

2.2.2.7 Synthesis of $[Cp^{*n\text{-}pentyl}IrCl]_2(\mu^2\text{-}Cl)_2$ **2g**

Following the general procedure, $[Ir(COD)]_2(\mu^2\text{-}Cl)_2$ (0.100 g, 0.149 mmol), $Cp^{*n\text{-}pentyl}$ (0.100 g, 0.521 mmol), and 0.5 mL of HCl were reacted in methanol (4 mL) to give **2g** (0.116 g, 85.7% yield). ^{1}H NMR (400 MHz, $CDCl_3$) δ 2.14 – 2.11 (t, 4H), 1.61 (s, 12 H), 1.59 (s, 12H), 1.43-1.29

(m, 12H), 0.88-0.85 (t, 6 H). ^{13}C NMR (101 MHz, $CDCl_3$) δ 88.23, 86.49, 86.46, 31.90, 27.43, 24.16, 22.48, 13.95, 9.51, 9.48.

HRMS/ESI+ (m/z): $C_{28}H_{46}[^{193}Ir]_2Cl_3$ 873.1924; Found 873.1965

Anal. Calc. for $C_{28}H_{46}Cl_4Ir_2$, C, 37.00; H, 5.10; Found, C, 37.60; H, 5.08

2.2.2.8 Synthesis of $[Cp^{*n\text{-hexyl}}IrCl]_2(\mu^2\text{-}Cl)_2$ **2h**

Following the general procedure, $[Ir(COD)]_2(\mu^2\text{-}Cl)_2$ (0.300 g, 0.447 mmol), $Cp^{*n\text{-hexyl}}$ (0.230 g, 1.12 mmol), and 0.5 mL of HCl were reacted in methanol (4 mL) to give **2h** (0.2367, 56.6% yield).^{1}H NMR (400 MHz, $CDCl_3$) δ 2.14 – 2.10 (t, 4H), 1.61 (s, 12 H), 1.59 (s, 12H), 1.40-1.24 (m, 16H), 0.88-0.85 (t, 6 H). ^{13}C NMR (101 MHz, $CDCl_3$) δ 88.34, 86.60, 86.56, 31.65, 29.53, 27.76, 24.26, 22.62, 14.16, 9.54, 9.51.

HRMS/ESI+ (m/z): $C_{30}H_{50}[^{193}Ir]_2Cl_3$ 901.2237; Found 901.2145

Anal. Calc. for $C_{30}H_{50}Cl_4Ir_2$, C, 38.46; H, 5.38; Found, C, 38.46; H, 5.38

2.2.2.9 Synthesis of $[Cp^{*n\text{-heptyl}}IrCl]_2(\mu^2\text{-}Cl)_2$ **2i**

Following the general procedure, $[Ir(COD)]_2(\mu^2\text{-}Cl)_2$ (0.250 g, 0.372 mmol), $Cp^{*n\text{-heptyl}}$ (0.287 g, 1.30 mmol), and 0.5 mL of HCl were reacted in methanol (4 mL) to give **2i** (0.168, 46.7% yield). ^{1}H NMR (400 MHz, $CDCl_3$) δ 2.14 – 2.10 (t, 4H), 1.60 (s, 12 H), 1.59 (s, 12H), 1.41-1.21 (m, 20H), 0.88-0.84 (t, 6 H). ^{13}C NMR (101 MHz, $CDCl_3$) δ 88.32, 86.59, 86.53, 31.82, 29.84, 29.18, 27.81, 24.27, 22.75, 14.23, 9.57, 9.52.

HRMS/ESI+ (m/z): $C_{32}H_{54}[^{193}Ir]_2Cl_3$ 929.2550; Found 929.2531

Anal. Calc. for $C_{32}H_{54}Cl_4Ir_2$, C, 39.83; H, 5.64; Found, C, 39.89; H, 5.60

2.2.2.10 Synthesis of $[Cp^{*n\text{-octyl}}IrCl]_2(\mu^2\text{-}Cl)_2$ **2j**

Following the general procedure, $[Ir(COD)]_2(\mu^2\text{-}Cl)_2$ (0.200 g, 0.298 mmol), $Cp^{*n\text{-octyl}}$ (0.349 g, 1.49 mmol), and 0.5 mL of HCl were reacted in methanol (4 mL) to give **2j** (0.246 g, 83.1% yield).

^{1}H NMR (400 MHz, $CDCl_3$) δ 2.14 – 2.10 (t, 4H), 1.61 (s, 12 H), 1.59 (s, 12H), 1.41-1.24 (m, 24H), 0.88-0.85 (t, 6 H). ^{13}C NMR (101 MHz, $CDCl_3$) δ 88.33, 86.60, 86.54, 31.95, 29.88, 29.47, 29.27, 27.81, 24.28, 22.78, 14.23, 9.58, 9.54.

HRMS/ESI+ (m/z): $C_{34}H_{58}[^{193}Ir]_2Cl_3$ 957.2863; Found 957.2828

Anal. Calc. for $C_{34}H_{58}Cl_4Ir_2$, C, 41.12; H, 5.89; Found, C, 41.28; H, 5.74

2.2.2.11 Synthesis of $[Cp^{*phenyl}IrCl]_2(\mu^2\text{-}Cl)_2$ **2k**

Following the general procedure, $[Ir(COD)]_2(\mu^2\text{-}Cl)_2$ (0.100 g, 0.149 mmol), $Cp^{*phenyl}$ (0.103 g, 0.521 mmol), and 0.5 mL of HCl were reacted in methanol (4 mL) to give **2k** (0.077 g, 48.8% yield). ^{1}H NMR (400 MHz, $CDCl_3$) δ 7.58 – 7.55 (m, 4H), 7.37 – 7.34 (m, 6H), 1.72 (s, 12 H), 1.63 (s, 12H). ^{13}C NMR (101 MHz, $CDCl_3$) δ 130.34, 129.94, 128.79, 128.58, 93.64, 85.61, 82.10, 10.50, 9.77.

HRMS/ESI+ (m/z): Calc. for $C_{30}H_{34}[^{193}Ir]_2Cl_3$ 885.0985; Found 885.1018

Anal. Calc. for $C_{30}H_{34}Ir_2Cl_4$, C, 39.13; H, 3.72; Found, C, 38.89; H, 3.51

2.2.2.12 Synthesis of $[Cp^{*benzyl}IrCl]_2(\mu^2\text{-}Cl)_2$ **2l**

Following the general procedure, $[Ir(COD)]_2(\mu^2\text{-}Cl)_2$ (0.100 g, 0.149 mmol), $Cp^{*benzyl}$ (0.111 g, 0.521 mmol), and 0.5 mL of HCl were reacted in methanol (4 mL) to give **2l** (0.123 g, 87.0% yield). ^{1}H NMR (400 MHz, $CDCl_3$) δ 7.30 – 7.27 (m, 2H), 7.26 – 7.25 (m, 2H), 7.23 – 7.18 (m, 2H), 7.11 – 7.09 (m, 4H), 3.57 (s, 4 H), 1.65 (s, 12 H), 1.63 (s, 12H). ^{13}C NMR (101 MHz, $CDCl_3$) δ 136.97, 128.88, 128.38, 126.90, 87.68, 86.90, 85.93, 30.58, 9.97, 9.53.

HRMS/ESI+ (m/z): Calc. for $C_{32}H_{38}[^{193}Ir]_2Cl_3$ 913.1298; Found 913.1347

Anal. Calc. for $C_{32}H_{38}Ir_2Cl_4$, C, 40.51; H, 4.04; Found, C, 40.40; H, 3.98

2.2.2.13 Synthesis of $[Cp^{*phenethyl}IrCl]_2(\mu^2\text{-}Cl)_2$ **2m**

Following the general procedure, $[Ir(COD)]_2(\mu^2\text{-}Cl)_2$ (0.200 g, 0.298 mmol), $Cp^{*phenethyl}$ (0.336 g, 1.49 mmol), and 0.5 mL of HCl were reacted in methanol (4 mL) to give **2m** (0.245 g, 84.2% yield). ^{1}H NMR (400 MHz, $CDCl_3$) δ 7.25 – 7.16 (m, 6H), 7.04 – 7.02 (m, 4H), 2.77 – 2.73 (t, 4H), 2.48 – 2.45 (t, 4H), 1.55 (s, 12 H), 1.36 (s, 12H). ^{13}C NMR (101 MHz, $CDCl_3$) δ 140.14, 128.64, 128.46, 126.35, 87.22, 86.30, 86.29, 33.60, 26.60, 9.27, 9.09.

HRMS/ESI+ (m/z): Calc. for $C_{34}H_{42}[^{193}Ir]_2Cl_3$ 941.1611; Found 941.1616

Anal. Calc. for $C_{34}H_{42}Ir_2Cl_4$, C, 41.80; H, 4.33; Found, C, 41.92; H, 4.22

2.2.2.14 Synthesis of $[Cp^{*cyclohexyl}IrCl]_2(\mu^2\text{-}Cl)_2$ **2n**

Following the general procedure, $[Ir(COD)]_2(\mu^2\text{-}Cl)_2$ (0.200 g, 0.298 mmol), $Cp^{*cyclohexyl}$ (0.152 g, 0.744 mmol), and 0.5 mL of HCl were reacted in methanol (4 mL) to give **2n** (0.079 g, 28.5% yield). ^{1}H NMR (400 MHz, $CDCl_3$) δ 2.08 – 2.01 (m, 2H), 1.93 – 1.89 (m, 4H), 1.78 – 1.74 (m, 4H), 1.67 (s, 12 H), 1.59 (s, 12H), 1.43 – 1.22 (m, 10H), 1.14 (tt, 2H). ^{13}C NMR (101 MHz, $CDCl_3$) δ 90.77, 85.99, 84.81, 35.75, 30.88, 27.10, 26.20, 10.70, 9.74.

HRMS/ESI+ (m/z): Calc. for $C_{30}H_{46}[^{193}Ir]_2Cl_3$ 897.1924; Found 897.1946

Anal. Calc. for $C_{30}H_{46}Ir_2Cl_4$, C, 38.62; H, 4.97; Found, C, 38.77; H, 4.92

2.2.2.15 Synthesis of $[Cp^{*cyclopentyl}IrCl]_2(\mu^2\text{-}Cl)_2$ **2o**

Following the general procedure, $[Ir(COD)]_2(\mu^2\text{-}Cl)_2$ (0.250 g, 0.372 mmol), $Cp^{*cyclopentyl}$ (0.248 g, 1.30 mmol), and 0.5 mL of HCl were reacted in methanol (4 mL) to give **2o** (0.213 g, 59.8% yield). ^{1}H NMR (400 MHz, $CDCl_3$) δ 2.63 – 2.54 (quin, 2H), 2.13 – 2.06 (m, 4H), 2.09 – 2.02 (m, 4H), 1.74 – 1.71 (m, 2H), 1. 68 (s, 12 H), 1.67 – 1.60 (m, 10H), 1.59 (s, 12H). ^{13}C NMR (101 MHz, $CDCl_3$) δ 89.60, 86.07, 85.92, 36.05, 31.34, 26.67, 10.46, 9.72.

HRMS/ESI+ (m/z): Calc. for $C_{28}H_{42}[^{193}Ir]_2Cl_3$ 869.1611; Found 869.1567

2.2.3 Synthesis for HCp^{*R} ligands

Unless otherwise stated, all reactions were conducted under an N_2 atmosphere.

2.2.3.1 General procedure of HCp^{*R} ligands

A solution of the respective Grignard reagent (18.1 mmol) in THF was added to a stirred solution of 2,3,4,5-tetramethyl-2-cyclopentenone (2.00 g, 15.2 mmol) in anhydrous THF (20 mL). The mixture was refluxed for 24 h, then cooled to 0 °C and quenched with HCl. This solution was warmed to room temperature and agitated for 2 h. The mixture was diluted with diethyl ether (30 mL), washed with water (3 x 30 mL), and the organic layer dried over $MgSO_4$. The products were concentrated under reduced pressure, and purified by column chromatography (Silica gel, hexanes) to afford the product and isomers as a yellow oil. The ^1H NMR spectra of the dienes are complex due to the signal overlap of the isomers.

2.2.3.2 Synthesis of 5-isopropyl-2,3,4,5-tetramethylcyclopenta-1,3-diene

Yield: 1.04 g (44%). This ligand has been previously characterized.[42]

2.2.3.3 Synthesis of 5-butyl-1,2,3,4-tetramethylcyclopenta-1,3-diene

Yield: 2.53 g (98%).

2.2.3.4 Synthesis of 5-isobutyl-1,2,3,4-tetramethylcyclopenta-1,3-diene

Yield: 2.49 g (96%).

HRMS/APCI+ (m/z): Calc. for $C_{13}H_{23}$ 179.1800; Found 179.1798

2.2.3.5 Synthesis of 5-(*sec*-butyl)-1,2,3,4-tetramethylcyclopenta-1,3-diene

Yield: 1.02 g (40%).

HRMS/APCI+ (m/z): Calc. for $C_{13}H_{23}$ 179.1800; Found 179.1794

2.2.3.6 Synthesis of 1,2,3,4-tetramethyl-5-pentylcyclopenta-1,3-diene

Yield: 1.76 g (63%).

HRMS/ESI+ (m/z): Calc. for $C_{14}H_{23}$ 191.1800; Found 191.1792

2.2.3.7 Synthesis of 5-hexyl-1,2,3,4-tetramethylcyclopenta-1,3-diene

Yield: 0.651 g (22%).

2.2.3.8 Synthesis of 5-heptyl-1,2,3,4-tetramethylcyclopenta-1,3-diene

Yield: 2.53 g (79%).

HRMS/APCI+ (m/z): Calc. for $C_{16}H_{29}$ 221.2269; Found 221.2264

2.2.3.9 Synthesis of 1,2,3,4-tetramethyl-5-octylcyclopenta-1,3-diene

Yield: 2.61g (77%). This ligand has been previously characterized.[42]

2.2.3.10 Synthesis of (2,3,4,5-tetramethylcyclopenta-2,4-dien-1-yl)benzene

Yield: 2.78 g (97%). This ligand has been previously characterized.[42]

2.2.3.11 Synthesis of ((2,3,4,5-tetramethylcyclopenta-2,4-dien-1-yl)methyl)benzene

Yield: 2.58 g (84%). This ligand has been previously characterized.[42]

2.2.3.12 Synthesis of (2-(2,3,4,5-tetramethylcyclopenta-2,4-dien-1-yl)ethyl)benzene

Yield: 2.51 g (77%).

HRMS/APCI+ (m/z): Calc. for $C_{17}H_{23}$ 227.1800; Found 227.1799

2.2.3.13 Synthesis of 2,3,4,5-tetramethyl[1,1'-bi(cyclopentane)]-2,4-diene

Yield: 1.57 g (57%).

HRMS/APCI+ (m/z): Calc. for $C_{14}H_{21}$ 191.1800; Found 191.1794

2.2.3.14 Synthesis of (2,3,4,5-tetramethylcyclopenta-2,4-dien-1-yl)cyclohexane

Yield: 2.18 g (74%). This ligand has been previously characterized.[42]

2.2.4 Experimental Crystallography

Unless otherwise stated, crystals were centered on the goniometer of a Rigaku Oxford Diffraction Gemini E Ultra diffractometer operating with MoKα radiation. The data collection routine, unit cell refinement, and data processing were carried out with the program CrysAlisPro.[1] The Laue symmetry and systematic absences were consistent with the monoclinic space group $P2_1/c$. The structure was solved using SHELXT-2014[2] and refined using SHELXL-2014[3] via Olex2.[4] The final refinement model involved anisotropic displacement parameters for non-hydrogen atoms and a riding model for all hydrogen atoms. Olex2 was used for molecular graphics generation. [5]

(1) CrysAlisPro Software System, v1.171.37.35, Rigaku Oxford Diffraction, **2015**, Rigaku Corporation, Oxford, UK.
(2) Sheldrick, G. M. "SHELXT – Integrated space-group and crystal structure determination." *Acta Cryst*. **2015**, *A71*, 3–8.
(3) Sheldrick, G. M. "A short history of SHELX." *Acta Cryst.* **2008**, *A64*, 112-122.
(4) Dolomanov, O.V.; Bourhis, L. J.; Gildea, R. J.; Howard, J. A. K.; Puschmann, H. *J. Appl. Cryst.* **2009**, ***42***, 339–341.
(5) Dolomanov, O.V.; Bourhis, L. J.; Gildea, R. J.; Howard, J. A. K.; Puschmann, H. *J. Appl. Cryst.* **2009**, ***42***, 339–341.

Chapter 3 Results and Discussion

3.1 Synthesis of modified Cp*^{R} ligands

The modified HCp*^{R} variants were synthesized via reaction of 1.25 molar equivalents of a Grignard reagent and 2,3,4,5-tetramethylcyclopent-2-enone in anhydrous THF. The resulting reaction produced an alcohol intermediate; subsequently, water was eliminated under acidic conditions to form the corresponding diene (**Figure 10**).

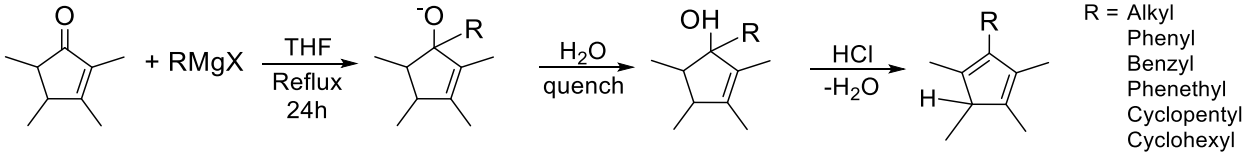

Figure 10. General scheme for the modification of HCp*^{R} ligands.

Purification of the final HCp*^{R} ligands was carried out via column chromatography on silica gel using hexanes as the eluent. The solvent was removed under reduced pressure to obtain the ligand as a yellow oil. The ^{1}H NMR spectra of the HCp*^{R} ligands are complex due to signal overlap of the multiple isomers (1-4, **Figure 11**).

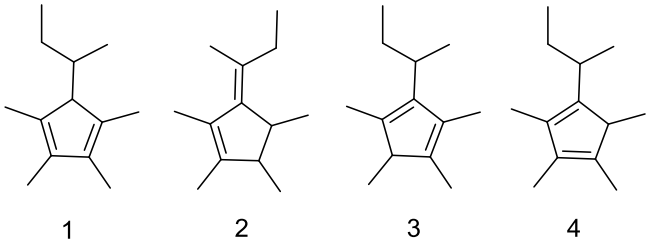

Figure 11. Potential isomers of Cp*$^{sec\text{-butyl}}$ precursor ligands formed through elimination of the alcohol intermediate.

Table 9. Percent yields of modified cyclopentadienyl ligands (**Figure 12**).

Entry	Ligand	Yield
1a	Isopropyl Cp*	44%
1b	*n*-butyl Cp*	98%
1c	Isobutyl Cp*	96%
1d	*sec*-butyl Cp*	40%
1e	*n*-pentyl Cp*	63%
1f	*n*-hexyl Cp*	22%
1g	*n*-heptyl Cp*	80%
1h	*n*-octyl Cp*	77%
2	Phenyl Cp*	97%
3	Benzyl Cp*	84%
4	Phenethyl Cp*	77%
5	Cyclohexyl Cp*	74%
6	Cyclopentyl Cp*	57%

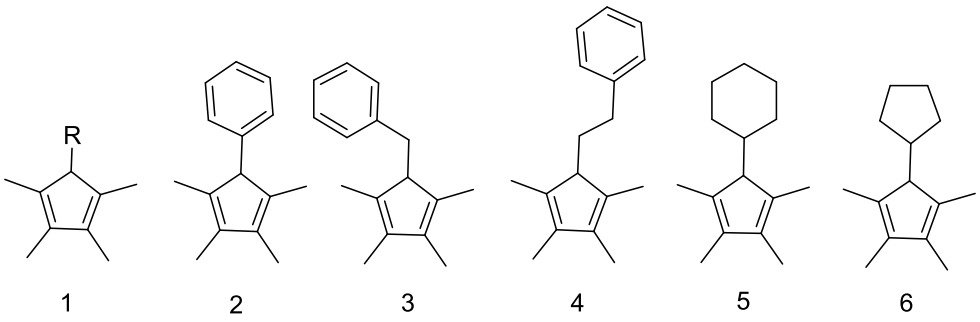

Figure 12. A list of the various HCp^{*R} ligands synthesized: (1a-1h) Cp^{*R}, (2) phenyl Cp*, (3) benzyl Cp*, (4) phenethyl Cp*, (5) cyclohexyl Cp*, (6) cyclopentyl Cp*.

3.2 Synthesis of $[Cp^*IrCl]_2(\mu^2\text{-}Cl)_2$ and $[Cp^*RhCl]_2(\mu^2\text{-}Cl)_2$ complexes

3.2.1 Microwave synthesis vs conventional synthesis

The synthesis of modified pentasubstituted cyclopentadienyl iridium and rhodium dimeric species was carried out using an adaptation of a previously reported literature procedure (**Figure 13**).[43] The reaction of $[M(COD)]_2(\mu^2\text{-}Cl)_2$ with 3.5-5 equivalents of the HCp^{*R} in the presence of HCl led to formation of the corresponding $[Cp^{*R}MCl]_2(\mu^2\text{-}Cl)_2$. The cyclopentadienyl dimeric

derivatives are formed by an electrophilic two-electron oxidative addition to each metal of $[M(COD)]_2(\mu^2\text{-}Cl)_2$ to give the intermediate as a $32e^-$ species $[MH(COD)Cl_2]_2$.[43] For rhodium, the resulting yellow suspension was microwaved for one hour to yield a red precipitate or a red solution. Similarly, for iridium, the resulting orange suspension formed an orange precipitate or an orange solution after being microwaved for 1 hour. In both syntheses, the solvent was removed under reduced pressure and the crude product was recrystallized from DCM and hexanes to yield the desired product as a red powder (Rh) or an orange powder (Ir). Each dimeric complex was characterized via ^1H NMR, ^{13}C NMR, ESI-MS, CH analysis, and X-ray crystallography, when possible.

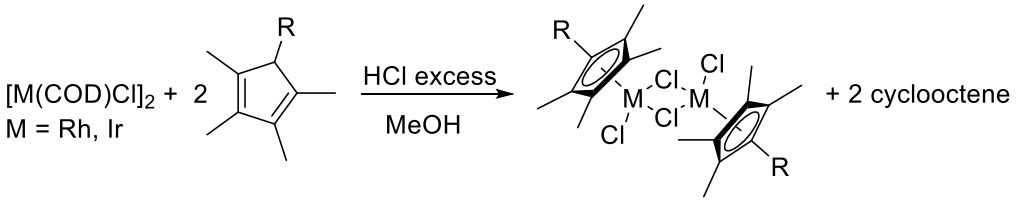

Figure 13. General scheme for the synthesis of $[Cp^{*R}MCl]_2(\mu^2\text{-}Cl)_2$ from $[M(COD)]_2(\mu^2\text{-}Cl)_2$ (M = Rh, Ir).

The iridium dimers were obtained in yields ranging from 48.7-95.7% (**Table 10**) whereas the rhodium dimers were obtained in yields ranging from 15.5-88.5%. Few rhodium complexes did not completely react, resulting in a lower yield for $Cp^{*isopropyl}$ (**Table 11**). This results suggests that $[Rh(COD)]_2(\mu^2\text{-}Cl)_2$ does not oxidize as readily as $[Ir(COD)]_2(\mu^2\text{-}Cl)_2$ as the rate of oxidation is slower than that of complex formation.

Table 10. Comparison of iridium dimers synthesized conventionally and with a microwave reactor.

Ligand	Conventional Yield[a]	Microwave Yield[b,c]	Overall Yield[d]
Ethyl Cp*	45.1%	50.0%	46.0%
Propyl Cp*	17.1%	61.4%	56.5%
Isopropyl Cp*	56.0%	69.9%	64.3%
Butyl Cp*	19.6%	55.3%	50.9%
Isobutyl Cp*	NR[d]	75.7%	69.7%
sec-Butyl Cp*	NR[d]	95.7%	88.1%
Pentyl Cp*	16.2%	85.7%	78.9%
Hexyl Cp*	9.05%	56.6%	52.0%
Heptyl Cp*	4.03%	46.7%	43.0%
Octyl Cp*	57.8%	83.1%	76.5%
Phenyl Cp*	30.0%	88.5%	81.4%
Benzyl Cp*	42.0%	87.0%	80.0%
Phenethyl Cp*	23.4%	84.2%	77.5%
Cyclohexyl Cp*	49.0%	48.3%	45.0%
Cyclopentyl Cp*	NR[d]	59.8%	55.0%

[a] Unless otherwise stated, the reaction was carried out using $IrCl_3 \cdot xH_2O$ and the corresponding ligand refluxed in MeOH for 48 h under N_2. [b] Unless otherwise stated, the reaction was carried out in a microwave pressure tube for 1 h. [c] Isolated yield. [d] No reaction. [e] Based on an 92% yield for $[Ir(COD)]_2(\mu^2\text{-}Cl)_2$.

Microwave-facilitated reaction of modified dienes with $[M(COD)]_2(\mu^2\text{-}Cl)_2$ showed a significantly improved yield in comparison to that obtained by conventional heating methods. The ^1H NMR pattern of the Cp^{*R} ligand is simplified when complexed to the metal. Modified dimers exhibit two singlets from the chemically non-equivalent methyl groups of the Cp* ring upon introduction of the R group, dissimilar to the typical $[Cp^*MCl]_2(\mu^2\text{-}Cl)_2$, which exhibits a singlet

for all methyl groups. In the case of *sec*-butyl, more peaks are seen due to the presence of a chiral center on the ligand. All complexes synthesized exhibited a typical piano stool arrangement with chloride bridges between the metal centers and a terminal chloride bound to the metal, similarly to other reported iridium and rhodium dimers.[6-7, 44]

Table 11. Comparison of various rhodium dimers synthesized conventionally and with a microwave reactor.

Ligand[a]	Conventional Yield[a]	Microwave Yield[b,c]	Overall Yield[e]
Ethyl Cp*	62.8%	79.0%	74.2%
Propyl Cp*	46.5%	80.0%	75.2%
Isopropyl Cp*	-	15.5% [d]	14.5%
Butyl Cp*	2.8%	63.1%	59.3%
Isobutyl Cp*	-	88.5%	83.2%
sec-Butyl Cp*	-	54.0%	50.8%
Pentyl Cp*	-	76.5%	71.9%
Hexyl Cp*	-	72.7%	68.3%
Heptyl Cp*	-	52.2%	49.0%
Octyl Cp*	-	52.3%	49.2%
Phenyl Cp*	27.6%	74.6%	70.2%
Benzyl Cp*	34.7%	88.5%	83.2%
Phenethyl Cp*	65.5%	76.7%	72.1%
Cyclohexyl Cp*	-	63.6%[d]	59.8%
Cyclopentyl Cp*	-	53.9%	50.7%

[a] Unless otherwise stated, the reaction was carried out using $RhCl_3 \cdot xH_2O$ and refluxed for 48 h under N_2. [b] Unless otherwise stated, the reaction was carried out in a microwave pressure tube for 1 h. [c] Isolated yield. [d] Reacted yield. [e] Based on an average of 94% yield for $[Rh(COD)]_2(\mu^2\text{-}Cl)_2$.

The conventional syntheses for rhodium dimers with long chains and saturated rings yielded numerous undesired and unidentifiable side products, and, consequently, gave low yields as the

product could not be isolated from impurities, despite great efforts. As a result, only rhodium dimers with short chains or conjugated rings were able to be successfully synthesized and purified via the conventional method. Modified cyclopentadienyl dimers synthesized via the alternative route between $[Rh(COD)]_2(\mu^2\text{-}Cl)_2$ and the appropriate HCp^{*R} did not experience any complications in purification. The difficulties encountered when following the conventional synthesis emphasize not only the importance of the alternative method in synthesizing difficult dimers, but also the efficiency and cost effectiveness. This new route lessens the number and amount of reagents used, involves less chromatography, and reduces the amount of rhodium and iridium metal lost during reactions.

3.3 Crystal structures of iridium and rhodium chloro-bridged dimers

Single crystal X-ray diffraction is much more than a molecule identification technique. This technique provides not only molecular connectivity, but also gives quantitative details of connectivity in the form of bond distances and angles. It is often the case that bond distance and angle information can be related to steric and electronic characteristics of the molecules studied. In this present work, the differences between molecules are subtle – the replacement of one methyl group of pentamethylcyclopentadienyl with another organic group. Thus, differences based upon electronic differences are predicted to be small and that indeed turns out to be the case. Differences based on steric factors may be larger, however it is not useful (and often dangerous) to draw conclusions about solution structures based on solid state information. Nevertheless, it is always important to build a body of information on classes of compounds because it is not clear from the outset when important features in chemistry (especially in catalysis) are noted than can be related to subtle differences in bond distances or angles.

The structural characterization of iridium and rhodium complexes containing bridging chloride ligands has been documented.[7a, 44a-44b] In all cases, the crystal structures indicated that analogous rhodium and iridium structures for any given ligand were isostructural. Majority of the pentasubstituted dimers belong to the monoclinic space group No. 14 ($P2_1/c$) with the exception of Cp*$^{n\text{-butyl}}$ and [Cp*$^{n\text{-propyl}}$RhCl]$_2$(μ^2-Cl)$_2$, which belonged to the triclinic space group No. 2 (*P*-1). In each dimeric complex, the metal was found to lie 1.75-1.76 Å from the plane of the Cp* ring. As expected, the asymmetric unit contained half of the dimeric structure for all compounds with the exception of [Cp*^{ethyl}RhCl]$_2$(μ^2-Cl)$_2$ due to disorder present on one of the Cp*^{ethyl} rings. The long distances between the two metal centers of each dimer indicate that metal-metal bonding is unlikely.

In the case of [Cp*^{ethyl}IrCl]$_2$(μ^2-Cl)$_2$ (**Figure 14**), the 2.4439(9)Å bond length of the Ir-Cl(B) is shorter than the 2.456(3)Å Ir-Cl(B) of [Cp*IrCl]$_2$(μ^2-Cl)$_2$.[44b] In addition, the Ir-Ir distance was found to be shorter (3.7025(5)Å vs 3.769(1)Å) for [Cp*^{ethyl}IrCl]$_2$(μ^2-Cl)$_2$. The similarities between the iridium structures arise from the bond distances of both the Ir-Cl(T) and Ir-C(centroid) (**Table 12**). In contrast, the angles of Ir-Cl(B)-Ir', Cl(B)-Ir-Cl(B'), and Cl(T)-Ir-Cl(B), are all unique with respect to [Cp*^{ethyl}IrCl]$_2$(μ^2-Cl)$_2$ (**Table 13**).

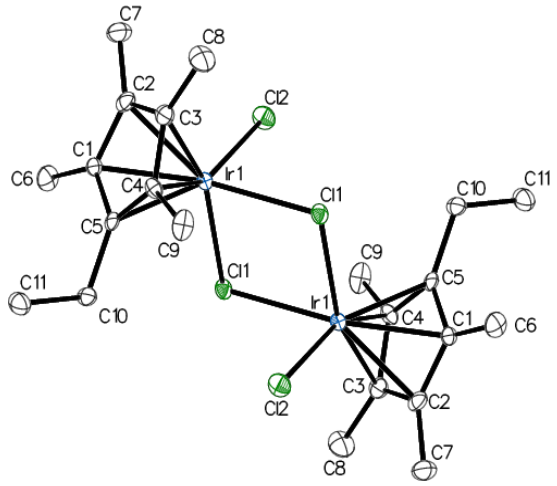

Figure 14. ADP Plot of $[Cp^{*ethyl}IrCl]_2(\mu^2\text{-}Cl)_2$. Hydrogen atoms omitted for clarity. Ellipsoids shown at 50% probability.

In comparison, $[Cp^{*ethyl}RhCl]_2(\mu^2\text{-}Cl)_2$ exhibits several differences as a result of disorder present on the Cp^{*ethyl} ring attached to Rh2 (**Figure 15**). In contrast to $[(Cp^{*ethyl})_2Rh(\mu\text{-}Cl)_3]PF_6^-$, the M-M bond distance is 3.216(1)Å, which is significantly shorter than the hexafluorophosphate salt, 3.7024(6)Å.[45] In addition, the dimeric complex also displays disorder over the chlorides and the anionic hexafluorophosphate. As a result, $[Cp^{*ethyl}RhCl]_2(\mu^2\text{-}Cl)_2$ contains unique bond lengths and angles when compared to both $[Cp^*RhCl]_2(\mu^2\text{-}Cl)_2$ and $[(Cp^{*ethyl})_2Rh(\mu\text{-}Cl)_3]PF_6^-$.

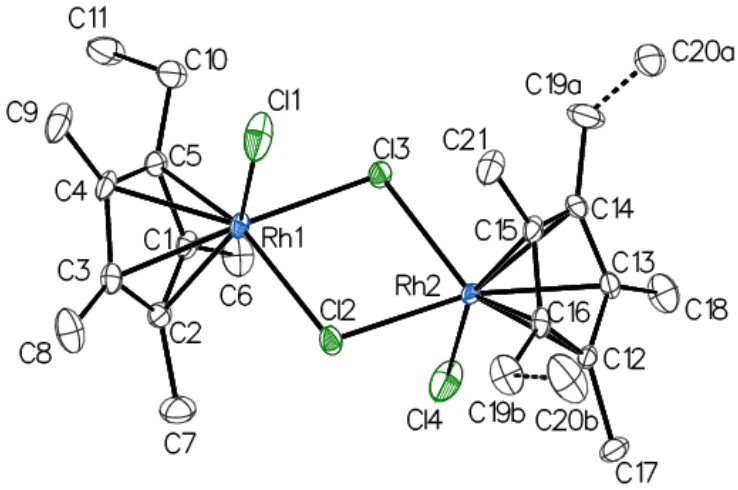

Figure 15. ADP Plot of $[Cp^{*ethyl}RhCl]_2(\mu^2\text{-}Cl)_2$. Hydrogen atoms omitted for clarity. Ellipsoids shown at 50% probability.

Table 12. Comparison of bond lengths of modified Cp*^{ethyl} and Cp*.

Measurement	Cp*	Cp*^{ethyl}	Measurement	Cp*	Cp*^{ethyl}
Ir-C(centroid)	1.7563(4)	1.7547(13)	Rh-C(centroid)	1.7558 (3)	1.7566(13)
Ir-Cl (T)	2.387(4)	2.3879(10)	Rh-Cl (T)	2.3967(11)	2.4102(8)
Ir-Cl(bridging)	2.456(3)	2.4439(9)	Rh-Cl(bridging)	2.4649(11)	2.4458(7)
Ir-Ir	3.769(1)	3.7025(5)	Rh-Rh	3.7191(6)	3.7024(6)

Table 13. Comparison of bond angles of modified Cp*^{ethyl} and Cp*.

Measurement	Cp*	Cp*^{ethyl}	Measurement	Cp*	Cp*^{ethyl}
Ir-Cl(B)-Ir'	100.45(12)	98.46(3)	Rh-Cl(B)-Rh'	98.29(3)	97.77(3)
Cl(B)-Ir-Cl(B)'	79.55(12)	81.54(3)	Cl(B)-Rh-Cl(B)'	81.71(3)	82.51(3)
Cl(T)-Ir-Cl(B)	89.65(12)	87.86(3)	Cl(T)-Rh-Cl(B)	92.30(4)	91.01(3)

As expected, the [Cp*$^{n\text{-propyl}}$IrCl]$_2$(μ^2-Cl)$_2$ (**Figure 16**) behaves similarly to the previous iridium structures and has C_i symmetry. The bond length of the Ir-Cl(B) is slightly longer than the Ir-Cl(B) of the [Cp*^{ethyl}IrCl]$_2$(μ^2-Cl)$_2$ (2.4486(6)Å vs 2.4439(9)Å). In addition, the Ir-Ir distance is longer (3.74982(17)Å vs 3.7025(5)Å) for [Cp*$^{n\text{-propyl}}$IrCl]$_2$(μ^2-Cl)$_2$. The similarities amongst iridium structures arise from the distances between the Ir-Cl(T) and Ir-C(centroid) (**Table 12**, **Table 14**). In contrast, the angles of Ir-Cl(B)-Ir', Cl(B)-Ir-Cl(B'), and Cl(T)-Ir-Cl(B), are all unique with respect to [Cp*$^{n\text{-propyl}}$IrCl]$_2$(μ^2-Cl)$_2$ (**Table 15**).

The space-filling model shows [Cp*$^{n\text{-propyl}}$IrCl]$_2$(μ^2-Cl)$_2$ (**Figure 17**) one dimer seated in between ten adjacent dimers and exhibits an alternating packing of the extended motif. The pattern involves a slight twist in the adjacent row of dimers due to the *n*-propyl chain, before a rearrangement is observed in the next row parallel to the first row. This phenomenon occurs as the *n*-propyl chain does not extend out into space, instead the *n*-propyl chain lies parallel to a neighboring Cp* ring. As evidenced by the powder pattern, the single crystal prediction matches the bulk powder, proving the bulk product does not contain additional isomorphs or other compounds.

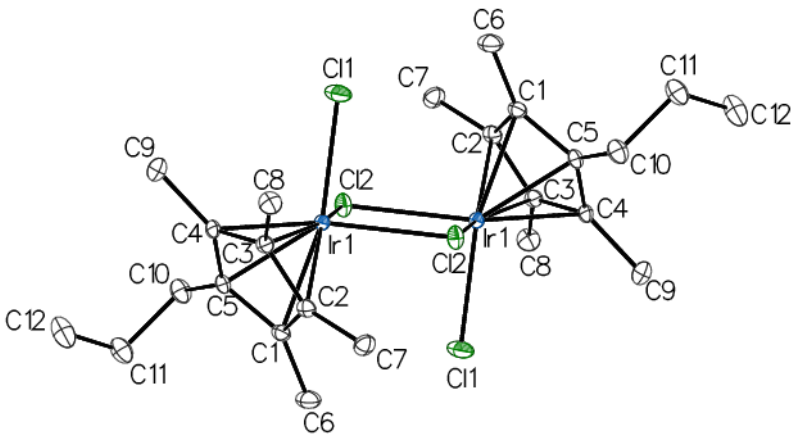

Figure 16. ADP Plot of $[Cp^{*n\text{-propyl}}IrCl]_2(\mu^2\text{-}Cl)_2$. Hydrogen atoms omitted for clarity. Ellipsoids shown at 50% probability. Previously reported by Morris *et al*.[46]

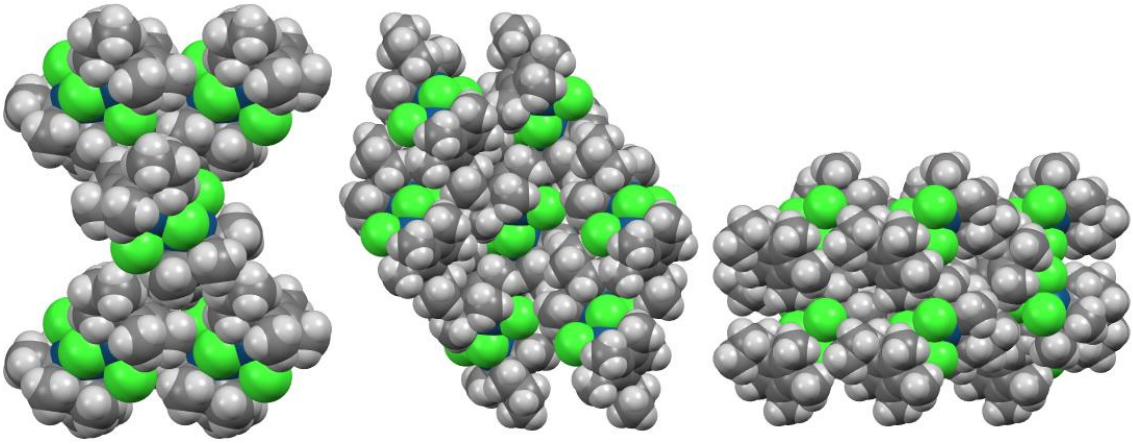

Figure 17. Space-filling model of $[Cp^{*n\text{-propyl}}IrCl]_2(\mu^2\text{-}Cl)_2$ down the a-axis (left), b-axis (middle), and c-axis (right).

$[Cp^{*n\text{-propyl}}RhCl]_2(\mu^2\text{-}Cl)_2$ (**Figure 18**, **Figure 19**) was found to be nearly identical to the iridium analogue. Like the iridium dimer, the pattern involves a slight twist in the neighboring row of dimers, before a readjustment in the next row parallel to the first row. The interactions present can be attributed to the *n*-propyl chain moving away from the Cp* ring. By using a structural overlay, it is clear that each dimeric complex displays similar features. The only difference lies in the M-M distance with the rhodium being shorter, resulting in a more acute M-Cl-M and Cl(T)-M-Cl(B) angle in contrast to the iridium analogue.

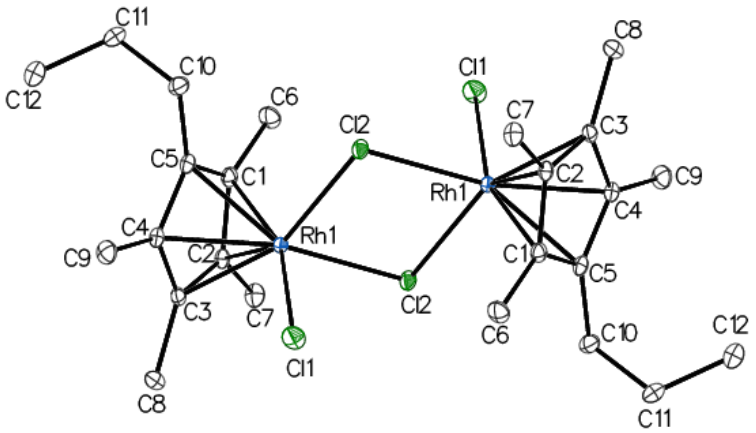

Figure 18. ADP Plot of $[Cp^{*n\text{-propyl}}RhCl]_2(\mu^2\text{-}Cl)_2$. Hydrogen atoms omitted for clarity. Ellipsoids shown at 50% probability.

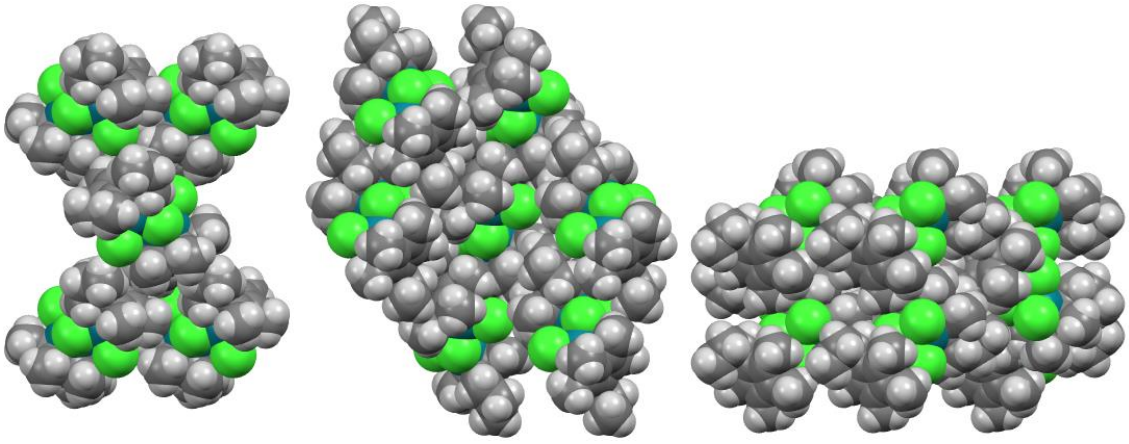

Figure 19. Space-filling model of $[Cp^{*n\text{-propyl}}RhCl]_2(\mu^2\text{-}Cl)_2$ down the a-axis (left), b-axis (middle), and c-axis (right).

Table 14. Comparison of bond lengths of modified $Cp^{*n\text{-propyl}}$ for iridium and rhodium.

Measurement	$Cp^{*n\text{-propyl}}$	Measurement	$Cp^{*n\text{-propyl}}$
Ir-C(centroid)	1.7541(13)	Rh-C(centroid)	1.7586(7)
Ir-Cl (T)	2.3925(10)	Rh-Cl (T)	2.4096(4)
Ir-Cl(bridging)	2.4486(6)	Rh-Cl(bridging)	2.4608(4)
Ir-Ir	3.74982(17)	Rh-Rh	3.7192(4)

Table 15. Comparison of bond angles of modified Cp*$^{n\text{-propyl}}$ for iridium and rhodium.

Measurement	Cp*$^{n\text{-propyl}}$	Measurement	Cp*$^{n\text{-propyl}}$
Ir-Cl(B)-Ir'	100.10(2)	Rh-Cl(B)-Rh'	98.405(13)
Cl(B)-Ir-Cl(B)'	79.90(2)	Cl(B)-Rh-Cl(B)'	81.595(13)
Cl(T)-Ir-Cl(B)	88.86(2)	Cl(T)-Rh-Cl(B)	92.288(14)

When the lattice forms with an included solvent molecule, the [Cp*$^{n\text{-propyl}}$RhCl]$_2$(μ^2-Cl)$_2$ crystallizes in a different space group (**Figure 20**). The dimer exhibits weak hydrogen bonding, 2.7708(6)Å and 2.7774(6)Å respectively, between the DCM molecule with both the terminal and bridging chloride. This complex behaves differently in space because of the solvent present in the lattice (**Figure 21**, **Figure 22**). With DCM present in the lattice, there is a shortened M-M distance of the rhodium atoms 3.6583(4)Å vs 3.7192(4)Å (**Table 18**). As a result, both the M-Cl-M and Cl-M-Cl angles are larger when compared to the dimeric complex without solvent (**Table 17**).

.

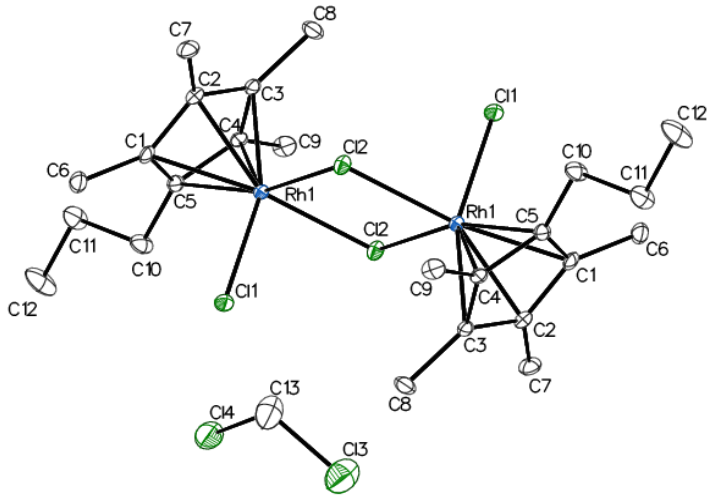

Figure 20. ADP Plot of [Cp*$^{n\text{-propyl}}$RhCl]$_2$(μ^2-Cl)$_2$ with a dichloromethane molecule. Hydrogen atoms omitted for clarity. Ellipsoids shown at 50% probability.

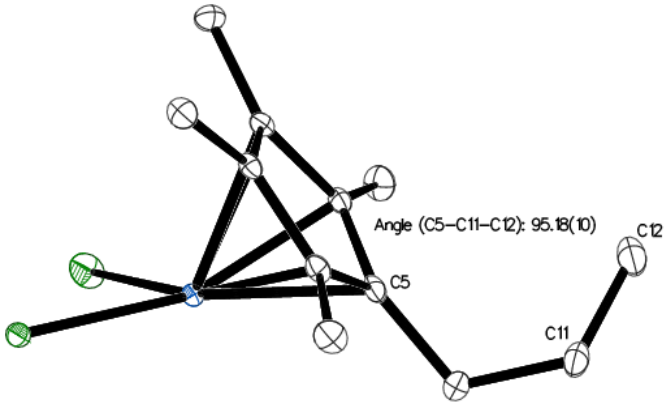

Figure 21. ADP Plot of the asymmetric unit for $[Cp^{*n\text{-propyl}}RhCl]_2(\mu^2\text{-}Cl)_2$ depicting the *n*-propyl chain behavior. Hydrogen atoms omitted for clarity. Ellipsoids shown at 50% probability.

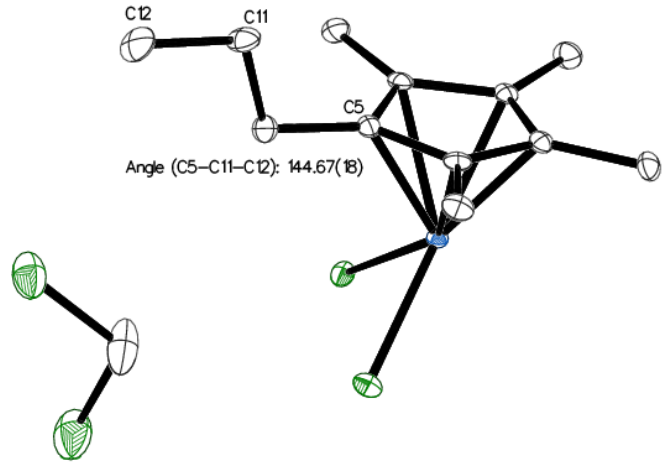

Figure 22. ADP Plot of the asymmetric unit for $[Cp^{*n\text{-propyl}}RhCl]_2(\mu^2\text{-}Cl)_2$ with DCM, depicting the *n*-propyl chain behavior. Hydrogen atoms omitted for clarity. Ellipsoids shown at 50% probability.

Table 16. Comparison of bond lengths of modified rhodium $Cp^{*n\text{-propyl}}$ with and without solvent.

Measurement	$Cp^{*n\text{-propyl w/DCM}}$	Measurement	$Cp^{*n\text{-propyl}}$
Rh-C(centroid)	1.7569(10)	Rh-C(centroid)	1.7586(7)
Rh-Cl (T)	2.4040(6)	Rh-Cl (T)	2.4096(4)
Rh-Cl(bridging)	2.4478(6)	Rh-Cl(bridging)	2.4608(4)
Rh-Rh	3.6583(4)	Rh-Rh	3.7192(4)

Table 17. Comparison of bond angles of modified rhodium Cp*$^{n\text{-propyl}}$ with and without solvent.

Measurement	Cp*$^{\text{n-propyl w/DCM}}$	Measurement	Cp*$^{\text{n-propyl}}$
Rh-Cl(B)-Rh'	96.53(2)	Rh-Cl(B)-Rh'	98.405(13)
Cl(B)-Rh-Cl(B)'	83.47(2)	Cl(B)-Rh-Cl(B)'	81.595(13)
Cl(T)-Rh-Cl(B)	89.53(2)	Cl(T)-Rh-Cl(B)	92.288(14)

In [Cp*$^{n\text{-butyl}}$IrCl]$_2$(μ^2-Cl)$_2$ (**Figure 23**), the bond length of the Ir-Cl(B) is slightly longer than the Ir-Cl(B) of the [Cp*$^{n\text{-propyl}}$IrCl]$_2$(μ^2-Cl)$_2$, 2.4518(9)Å vs 2.4486(6)Å. In addition, the Ir-Ir distance is longer (3.7803(4)Å vs 3.74982(17)Å) for [Cp*$^{n\text{-propyl}}$IrCl]$_2$(μ^2-Cl)$_2$. The similarities of the iridium structures are best seen in the distances between the Ir-Cl(T) and Ir-C(centroid) (**Table 14**, **Table 18**). In contrast, the angles of Ir-Cl(B)-Ir', Cl(B)-Ir-Cl(B'), and Cl(T)-Ir-Cl(B), are all unique with respect to [Cp*$^{n\text{-butyl}}$IrCl]$_2$(μ^2-Cl)$_2$ (**Table 19**).

The space-filling model shows that [Cp*$^{n\text{-butyl}}$IrCl]$_2$(μ^2-Cl)$_2$ has a methyl moiety from each Cp* ring contain a close H-Cl interaction with a bridging chloride and has each Cp* ring oriented 180° to the other. As the *n*-butyl chain does not extend out into space, an alignment of the *n*-butyl chain is observed parallel with a neighboring *n*-butyl chain. Lastly, an H11 and H13 from neighboring *n*-butyl chains have short contact interactions between adjacent dimers. It is apparent that the *n*-butyl chain plays a significant role in how the iridium dimer packs, unlike its rhodium counterpart discussed below.

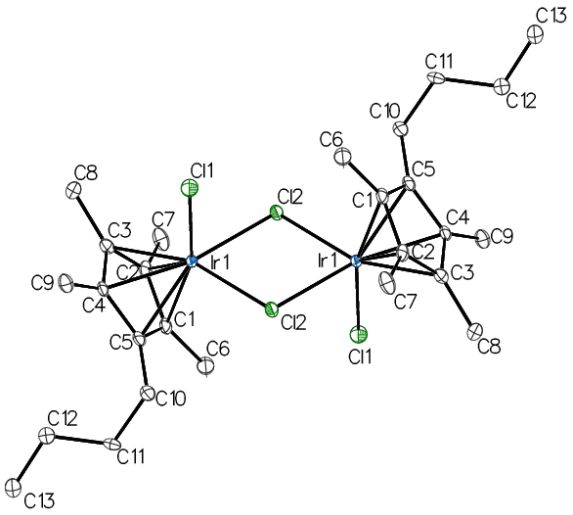

Figure 23. ADP Plot of $[Cp^{*n\text{-butyl}}IrCl]_2(\mu^2\text{-}Cl)_2$. Hydrogen atoms omitted for clarity. Ellipsoids shown at 50% probability.

The isostructural $[Cp^{*n\text{-butyl}}RhCl]_2(\mu^2\text{-}Cl)_2$ (**Figure 24**) does not exhibit short H-Cl contact interactions, even though a similar pattern is observed to the iridium analogue. Moreover, the difference between the dimeric structures can be seen within the bond angles of Cl(T)-M-Cl(B) and Cl(B)-M-Cl(B') with rhodium having larger angles (**Table 19**).

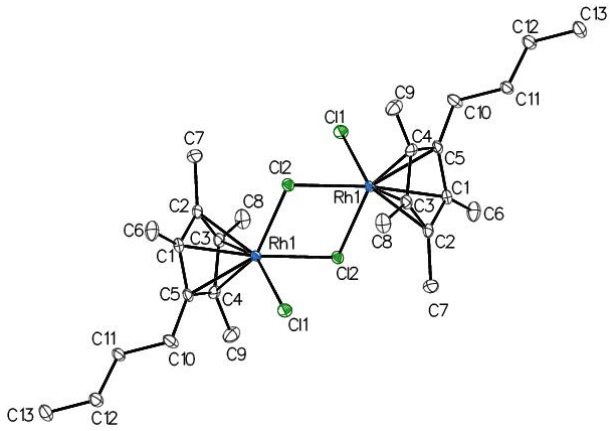

Figure 24. ADP Plot of $[Cp^{*n\text{-butyl}}RhCl]_2(\mu^2\text{-}Cl)_2$. Hydrogen atoms omitted for clarity. Ellipsoids shown at 50% probability.

Each $Cp^{*n\text{-butyl}}$ dimer exhibits varying *n*-butyl chain behavior. The rhodium $Cp^{*n\text{-butyl}}$ dimer shows the *n*-butyl chain extending away from the metal, displaying a typical 109.42° angle for an

sp^3 carbon adjacent to the Cp* ring. The distance between the Cp* ring C5 to C12 of the *n*-butyl chain is 3.860Å and has a torsion angle of 64.7(4)° (**Figure 25**). In contrast, the iridium Cp*$^{n\text{-butyl}}$ dimer shows the *n*-butyl chain folds back towards the Cp* ring and shows a 111.9° angle for the sp^3 carbon C10.

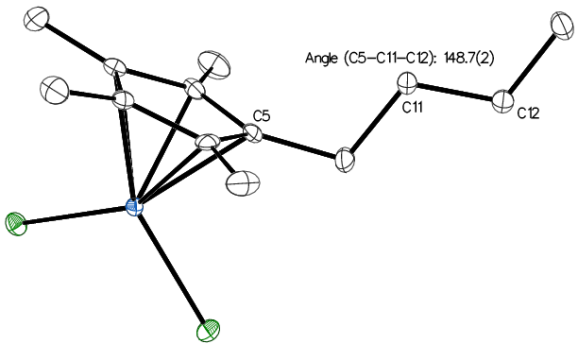

Figure 25. ADP Plot of the asymmetric unit for [Cp*$^{n\text{-butyl}}$RhCl]$_2$(μ^2-Cl)$_2$ depicting the *n*-butyl chain behavior. Hydrogen atoms omitted for clarity. Ellipsoids shown at 50% probability.

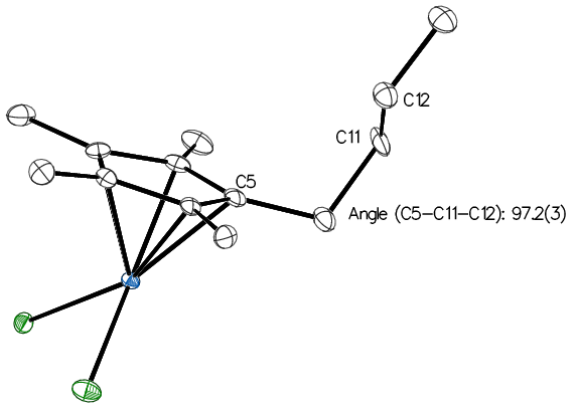

Figure 26. ADP Plot of the asymmetric unit for [Cp*$^{n\text{-butyl}}$IrCl]$_2$(μ^2-Cl)$_2$ depicting the *n*-butyl chain behavior. Hydrogen atoms omitted for clarity. Ellipsoids shown at 50% probability.

Table 18. Comparison of bond lengths of modified Cp*$^{n\text{-butyl}}$ for iridium and rhodium.

Measurement	Cp*$^{n\text{-butyl}}$	Measurement	Cp*$^{n\text{-butyl}}$
Ir-C(centroid)	1.7591(18)	Rh-C(centroid)	1.7511(14)
Ir-Cl (T)	2.3912(10)	Rh-Cl (T)	2.3973(8)
Ir-Cl(bridging)	2.4518(9)	Rh-Cl(bridging)	2.4642(8)
Ir-Ir	3.7803(5)	Rh-Rh	3.6174(6)

Table 19. Comparison of bond angles of modified Cp*$^{n\text{-butyl}}$ for iridium and rhodium.

Measurement	Cp*$^{n\text{-butyl}}$	Measurement	Cp*$^{n\text{-butyl}}$
Ir-Cl(B)-Ir'	100.63(3)	Rh-Cl(B)-Rh'	94.25(3)
Cl(B)-Ir-Cl(B)'	79.37(3)	Cl(B)-Rh-Cl(B)'	85.75(3)
Cl(T)-Ir-Cl(B)	89.31(3)	Cl(T)-Rh-Cl(B)	89.62(3)

As evidenced by [Cp*^{isobutyl}IrCl]$_2$(μ^2-Cl)$_2$ (**Figure 27**), the bond length of the Ir-Cl(B) is similar to the Ir-Cl(B) of the [Cp*$^{n\text{-butyl}}$IrCl]$_2$(μ^2-Cl)$_2$, 2.4512(10)Å vs 2.4518(9)Å. In addition, the Ir-Ir distance is shorter (3.6844(6)Å vs 3.7803(4)Å) for [Cp*$^{n\text{-butyl}}$IrCl]$_2$(μ^2-Cl)$_2$. The similarities between the iridium structures arise from the distances between the Ir-Cl(T) and Ir-C(centroid) (**Table 18**, **Table 20**). In contrast, the angles of Ir-Cl(B)-Ir', Cl(B)-Ir-Cl(B'), and Cl(T)-Ir-Cl(B), are all unique with respect to [Cp*$^{n\text{-butyl}}$IrCl]$_2$(μ^2-Cl)$_2$ (**Table 21**).

It is apparent from the space-filling model that [Cp*^{isobutyl}IrCl]$_2$(μ^2-Cl)$_2$ displays a pattern involving a twist in the adjacent row of dimers due to the isobutyl moiety. Similar to the *n*-propyl chain, the isobutyl group does not extend out into space, instead it aligns parallel with a neighboring Cp* ring.

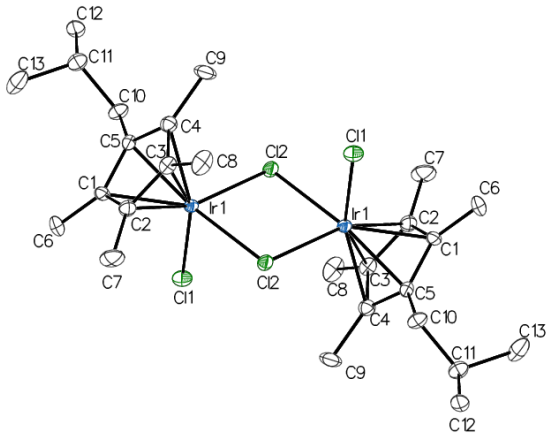

Figure 27. ADP Plot of [Cp*^{isobutyl}IrCl]$_2$(μ^2-Cl)$_2$. Hydrogen atoms omitted for clarity. Ellipsoids shown at 50% probability.

Table 20. Comparison of bond lengths of modified Cp*^{isobutyl} for iridium and rhodium.

Measurement	Cp*^{isobutyl}	Measurement	Cp*^{isobutyl}
Ir-C(centroid)	1.7489(18)	Rh-C(centroid)	1.7490(6)
Ir-Cl (T)	2.3902(11)	Rh-Cl (T)	2.3926(4)
Ir-Cl(bridging)	2.4512(10)	Rh-Cl(bridging)	2.4529(3)
Ir-Ir	3.6844(6)	Rh-Rh	3.5948(6)

Table 21. Comparison of bond angles of modified Cp*^{isobutyl} for iridium and rhodium.

Measurement	Cp*^{isobutyl}	Measurement	Cp*^{isobutyl}
Ir-Cl(B)-Ir'	97.48(3)	Rh-Cl(B)-Rh'	94.161(11)
Cl(B)-Ir-Cl(B)'	82.52(3)	Cl(B)-Rh-Cl(B)'	85.839(11)
Cl(T)-Ir-Cl(B)	87.93(4)	Cl(T)-Rh-Cl(B)	89.561(12)

In contrast, [Cp*^{isobutyl}RhCl]$_2$(μ^2-Cl)$_2$ (**Figure 28**) does not exhibit short contacts and packs in the unit cell with as little interaction as possible. The lack of interactions suggest that the iridium dimeric species packs more efficiently than its rhodium counterpart. The M-M distance is shorter in comparison to iridium (3.5948(6)Å vs 3.6844(6)Å) resulting in more acute angles for M-Cl-M and Cl(T)-M-Cl(B).

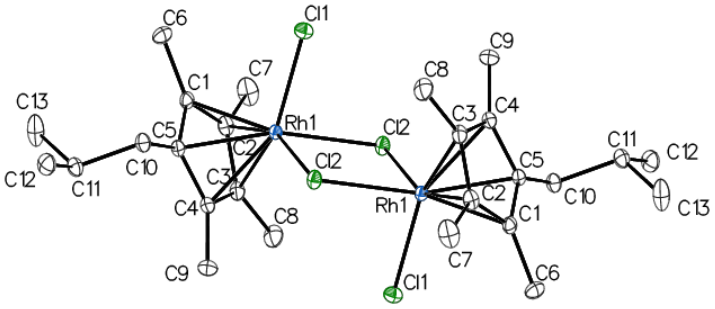

Figure 28. ADP Plot of [Cp*^{isobutyl}RhCl]$_2$(μ^2-Cl)$_2$. Hydrogen atoms omitted for clarity. Ellipsoids shown at 50% probability.

In the case of [Cp*$^{n\text{-pentyl}}$IrCl]$_2$(μ^2-Cl)$_2$ (**Figure 29**), the bond length of the Ir-Cl(B) is slightly longer than the Ir-Cl(B) of the [Cp*$^{n\text{-butyl}}$IrCl]$_2$(μ^2-Cl)$_2$, 2.4541(9)Å vs 2.4518(9)Å. In addition, the Ir-Ir distance is shorter (3.7371(6)Å vs 3.7803(4)Å) for [Cp*$^{n\text{-butyl}}$IrCl]$_2$(μ^2-Cl)$_2$. The

similarities among the iridium structures arise from the distances between the Ir-Cl(T) and Ir-C(centroid) (**Table 18**, **Table 22**). In contrast, the angles of Ir-Cl(B)-Ir', Cl(B)-Ir-Cl(B'), and Cl(T)-Ir-Cl(B), are all unique with respect to $[Cp^{*n\text{-butyl}}IrCl]_2(\mu^2\text{-}Cl)_2$ (**Table 23**).

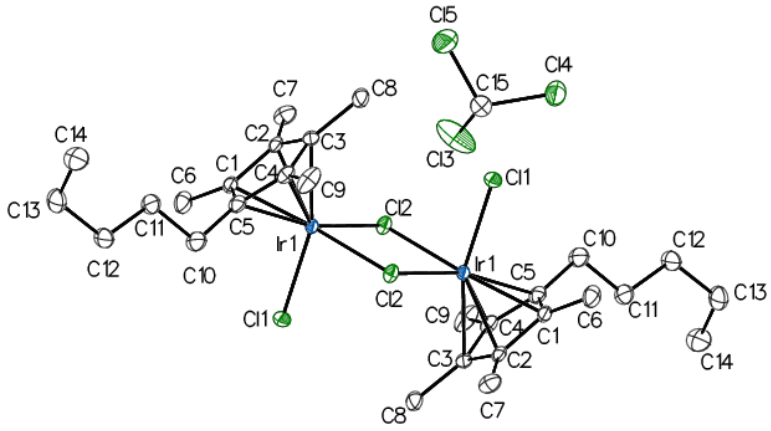

Figure 29. ADP Plot of $[Cp^{*n\text{-pentyl}}IrCl]_2(\mu^2\text{-}Cl)_2$. Hydrogen atoms omitted for clarity. Ellipsoids shown at 50% probability.

By observing the space-filling model of $[Cp^{*n\text{-pentyl}}IrCl]_2(\mu^2\text{-}Cl)_2$ (**Figure 30**) an oscillating pattern is noticed with two chloroform molecules present amid adjacent dimers. In addition, the two chloroform molecules alternate with the *n*-pentyl chain between each dimer. As a result, the dimer exhibits only chloride interactions with neighboring complexes. The terminal chloride exhibits weak hydrogen bonding (2.4971(9)Å) with the hydrogen, H15, on the chloroform molecule.

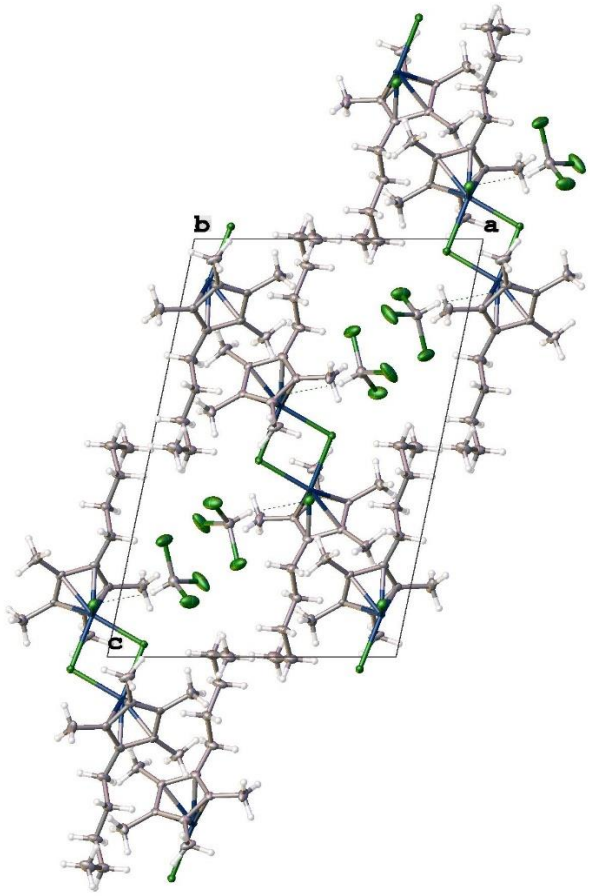

Figure 30. Model of $[Cp^{*n\text{-pentyl}}IrCl]_2(\mu^2\text{-}Cl)_2$ showing chloroform molecules between dimers. Ellipsoids shown at 50% probability.

The $[Cp^{*n\text{-pentyl}}RhCl]_2(\mu^2\text{-}Cl)_2$ (**Figure 31**) displays an oscillating pattern with two chloroform molecules among the adjacent dimers. In addition, the two chloroform molecules alternate with the *n*-pentyl chain between each dimer. The rhodium dimer exhibits chloride interactions with adjacent complexes via the terminal chloride that exhibits a weak hydrogen bond (2.4894(6)Å) with the hydrogen on the chloroform molecule. Lastly, Cl3 interacts with a neighboring Cl5 on a separate chloroform molecule to form a row of solvent between each dimer. By using a structural overlay, both dimeric complexes display similar features. The difference lies between the M-M distances with the rhodium dimer being shorter, resulting in a more acute M-Cl-M angle in contrast to the iridium analogue.

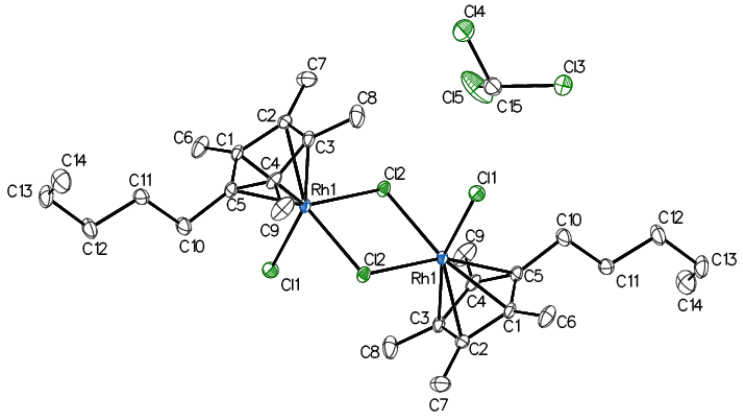

Figure 31. ADP Plot of $[Cp^{*n\text{-pentyl}}RhCl]_2(\mu^2\text{-}Cl)_2$. Hydrogen atoms omitted for clarity. Ellipsoids shown at 50% probability.

Table 22. Comparison of bond lengths of modified $Cp^{*n\text{-pentyl}}$ for iridium and rhodium.

Measurement	$Cp^{*n\text{-pentyl}}$	Measurement	$Cp^{*n\text{-pentyl}}$
Ir-C(centroid)	1.7579(16)	Rh-C(centroid)	1.7557(9)
Ir-Cl (T)	2.4041(9)	Rh-Cl (T)	2.4102(5)
Ir-Cl(bridging)	2.4541(9)	Rh-Cl(bridging)	2.4489(5)
Ir-Ir	3.7371(6)	Rh-Rh	3.6782(6)

Table 23. Comparison of bond angles of modified $Cp^{*n\text{-pentyl}}$ for iridium and rhodium.

Measurement	$Cp^{*n\text{-pentyl}}$	Measurement	$Cp^{*n\text{-pentyl}}$
Ir-Cl(B)-Ir'	99.41(3)	Rh-Cl(B)-Rh'	97.123(19)
Cl(B)-Ir-Cl(B)'	80.59(3)	Cl(B)-Rh-Cl(B)'	82.8876(19)
Cl(T)-Ir-Cl(B)	88.20(3)	Cl(T)-Rh-Cl(B)	90.832(18)

The crystal structures of both iridium and rhodium $Cp^{*benzyl}$, show each dimeric complex has a unit cell that appears either tetragonal or orthorhombic. However, each complex contains a 2-fold rotation, a glide plane, and inversion center (C_i) concluding that this complex is indeed monoclinic. The $Cp^{*benzyl}$ structures lack the π-π stacking interactions as seen in Sadler's $[Cp^{*phenyl}IrCl]_2(\mu^2\text{-}Cl)_2$ centroids of the phenyl systems (3.956Å),[7a] proving the benzyl moiety is not as rigid and has more freedom to rotate in space.

As exhibited by $[Cp^{*benzyl}IrCl]_2(\mu^2\text{-}Cl)_2$ (**Figure 32**), the bond length of the Ir-Cl(B) is longer than the Ir-Cl(B) of the $[Cp^{*phenyl}IrCl]_2(\mu^2\text{-}Cl)_2$, 2.4549(7)Å vs 2.4378(8)Å.[7a] In addition, the Ir-Ir distance is slightly shorter (3.7107(3)Å vs 3.7157(4)Å) for $[Cp^{*benzyl}IrCl]_2(\mu^2\text{-}Cl)_2$. The similarities between each iridium structure arises from the distances between the Ir-Cl(T) and Ir-C(centroid). In contrast, the angles of Ir-Cl(B)-Ir', Cl(B)-Ir-Cl(B'), and Cl(T)-Ir-Cl(B), are all unique with respect to $[Cp^{*phenyl}IrCl]_2(\mu^2\text{-}Cl)$.

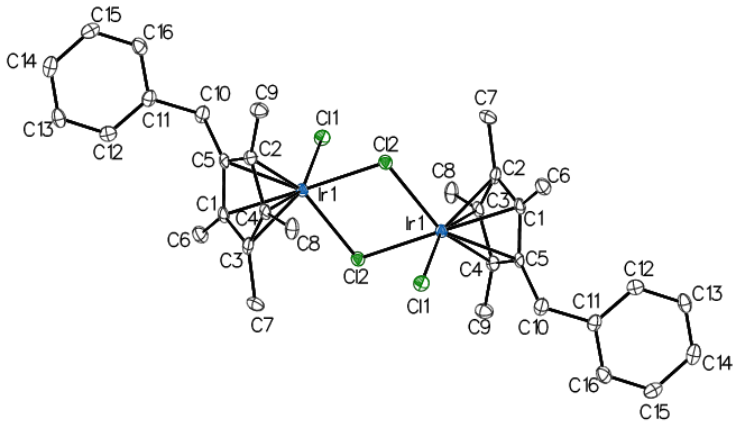

Figure 32. ADP Plot of $[Cp^{*benzyl}IrCl]_2(\mu^2\text{-}Cl)_2$. Hydrogen atoms omitted for clarity. Ellipsoids shown at 50% probability. Previously reported by Morris *et al*.[46]

The $[Cp^{*benzyl}RhCl]_2(\mu^2\text{-}Cl)_2$ (**Figure 33**) has a benzyl moiety that forces an adjacent dimer's Cp* ring to be perpendicular to the other Cp* ring. In comparison to the iridium complex, the bond lengths between the M-Cl(T) and M-Cl(B) were found to be identical (**Table 24)**. The difference between the structures are observed within the bond angles of Cl-M-Cl' and Cl(T)-M-Cl(B) with rhodium having larger angles (**Table 25**). In addition, the Ir-Ir distance is longer than the Rh-Rh distance, 3.7107(3)Å vs. 3.6502(8)Å respectively.

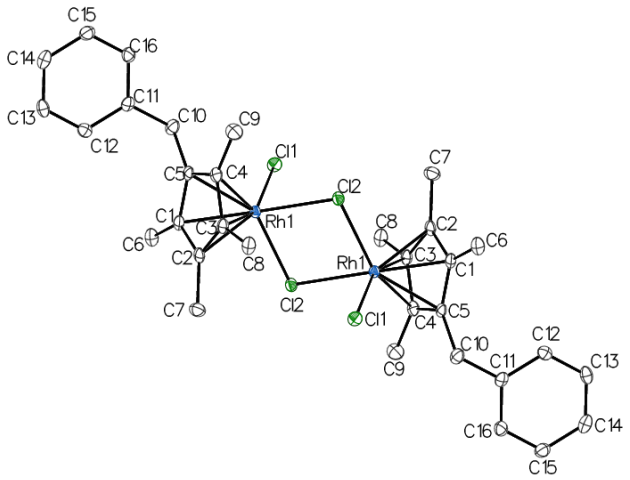

Figure 33. ADP Plot of $[Cp^{*benzyl}RhCl]_2(\mu^2\text{-}Cl)_2$. Hydrogen atoms omitted for clarity. Ellipsoids shown at 50% probability.

Table 24. Comparison of bond lengths of modified $Cp^{*benzyl}$ for iridium and rhodium.

Measurement	$Cp^{*benzyl}$	Measurement	$Cp^{*benzyl}$
Ir-C(centroid)	1.74621(8)	Rh-C(centroid)	1.7533(11)
Ir-Cl (T)	2.3914(7)	Rh-Cl (T)	2.3984(6)
Ir-Cl(bridging)	2.4549(7)	Rh-Cl(bridging)	2.4553(6)
Ir-Ir	3.7107(3)	Rh-Rh	3.6502(8)

Table 25. Comparison of bond angles of modified $Cp^{*benzyl}$ for iridium and rhodium.

Measurement	$Cp^{*benzyl}$	Measurement	$Cp^{*benzyl}$
Ir-Cl(B)-Ir'	98.19(4)	Rh-Cl(B)-Rh'	95.43(2)
Cl(B)-Ir-Cl(B)'	81.81(4)	Cl(B)-Rh-Cl(B)'	84.568(19)
Cl(T)-Ir-Cl(B)	87.73(4)	Cl(T)-Rh-Cl(B)	90.08(2)

As demonstrated by $[Cp^{*phenethyl}IrCl]_2(\mu^2\text{-}Cl)_2$, the bond length of the Ir-Cl(B) is slightly longer than the bond length of $[Cp^{*benzyl}IrCl]_2(\mu^2\text{-}Cl)_2$, 2.4567(7)Å vs 2.4549(7)Å. In addition, the Ir-Ir distance and Ir-C(centroid) is longer for $[Cp^{*phenethyl}IrCl]_2(\mu^2\text{-}Cl)_2$. The similarity between the iridium structures arise from the distance of the Ir-Cl(T) bond (**Table 24**, **Table 26**). In contrast, the angles of Ir-Cl(B)-Ir', Cl(B)-Ir-Cl(B'), and Cl(T)-Ir-Cl(B), are all unique with respect to $[Cp^{*benzyl}IrCl]_2(\mu^2\text{-}Cl)_2$.

It is apparent from the space-filling model that the $[Cp^{*phenethyl}IrCl]_2(\mu^2\text{-}Cl)_2$ (**Figure 34**) complex does not exhibit π-π stacking between the centroids of the phenyl systems nor the Cp* ring. The bond lengths between the M-Cl(T) and M-Cl(B) are identical as evidenced by **Table 26**. The difference between the structures is within the bond angles of Cl-M-Cl and M-Cl-M with rhodium having larger angles (**Table 27**). In the case of $[Cp^{*phenethyl}IrCl]_2(\mu^2\text{-}Cl)_2$, the bond length of the Ir-Cl(B) is unique to the bond length of the Rh-Cl(B) in $[Cp^{*phenethyl}RhCl]_2(\mu^2\text{-}Cl)_2$, 2.4567(7)Å vs 2.4586(4)Å. In addition, the Ir-Ir distance is longer than the Rh-Rh distance, 3.7446(5)Å and 3.6811(5) respectively. In contrast, each bond length and each angle is unique to the iridium and rhodium analogues.

The space-filling model of the iridium complex shows that the phenyl moiety has a C-C interaction with the Cp* ring on the neighboring molecule between C2 and C14. In addition, C13 interacts with an H11 on the CH_2 moiety of a neighboring phenethyl group. Additionally, an H7 and C2 interact with a C13 and C14 respectively on a neighboring phenethyl group. As evidenced by the powder pattern, the single crystal prediction matches the bulk powder, proving the dimeric complex does not contain additional isomorphs or crystalline defects.

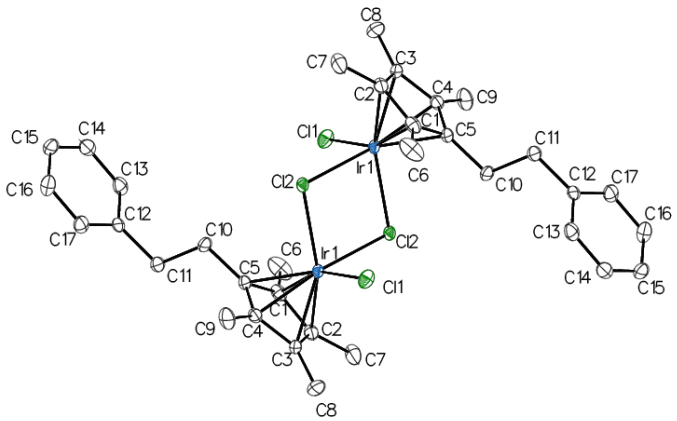

Figure 34. ADP Plot of $[Cp^{*phenethyl}IrCl]_2(\mu^2\text{-}Cl)_2$. Hydrogen atoms omitted for clarity. Ellipsoids shown at 50% probability.

The rhodium complex (**Figure 35**) contains similar interactions to the iridium analogue with the exception of the terminal chloride. The terminal chloride interacts with the CH_2 moiety instead of the C13 like with the iridium analogue.

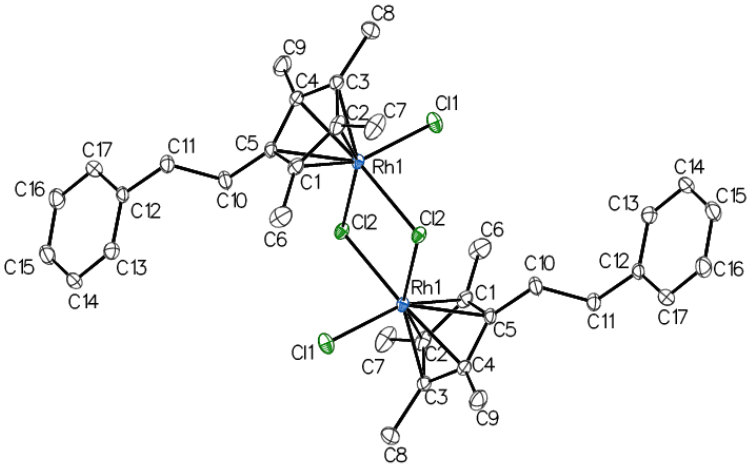

Figure 35. ADP Plot of $[Cp^{*phenethyl}RhCl]_2(\mu^2\text{-}Cl)_2$. Hydrogen atoms omitted for clarity. Ellipsoids shown at 50% probability.

Table 26. Comparison of bond lengths of modified $Cp^{*phenethyl}$ for iridium and rhodium.

Measurement	$Cp^{*phenethyl}$	Measurement	$Cp^{*phenethyl}$
Ir-C(centroid)	1.7531(12)	Rh-C(centroid)	1.7486(7)
Ir-Cl (T)	2.3919(8)	Rh-Cl (T)	2.3947(6)
Ir-Cl(bridging)	2.4567(7)	Rh-Cl(bridging)	2.4586(4)
Ir-Ir	3.74465(5)	Rh-Rh	3.6811(5)

Table 27. Comparison of bond angles of modified $Cp^{*phenethyl}$ for iridium and rhodium.

Measurement	$Cp^{*phenethyl}$	Measurement	$Cp^{*phenethyl}$
Ir-Cl(B)-Ir'	99.24(2)	Rh-Cl(B)-Rh'	96.811(14)
Cl(B)-Ir-Cl(B)'	80.77(2)	Cl(B)-Rh-Cl(B)'	83.189(14)
Cl(T)-Ir-Cl(B)	88.86(3)	Cl(T)-Rh-Cl(B)	91.146(15)

Examination of the various iridium dimers reveals little to no difference between the Ir-C and the Ir-Cl(bridging) bond distances; however, a slight increase in the bond distance of the Ir-Cl(T) is observed from Cp* to $Cp^{*n\text{-pentyl}}$. In addition, the Ir-Ir distance experiences a decrease

from that of $[Cp^*IrCl]_2(\mu^2\text{-}Cl)_2$. The Ir-Ir distance increases as the chain length increases from ethyl to *n*-butyl. With the exception of *n*-butyl, as the length of the alkyl chain increases, the Ir-Ir distance is less than that of $[Cp^*IrCl]_2(\mu^2\text{-}Cl)_2$, 3.769(1)Å. A similar trend is observed with the modified ring Cp^{*R} variants. The $Cp^{*phenyl}$ bond length of 3.7157(4)Å has a longer Ir-Ir distance than $Cp^{*benzyl}$. Likewise, there is an increase in Ir-Ir distance from $Cp^{*benzyl}$ to $Cp^{*phenethyl}$, similar to that of Cp^{*ethyl} and $Cp^{*n\text{-propyl}}$.

Table 28. Comparison of bond lengths for unmodified and modified Cp* chains for iridium.

Ligand	Ir-C(centroid)	Ir-Cl (T)	Ir-Cl(bridging)	Ir-Ir
Cp*	1.7563(4)	2.387(4)	2.456(3)	3.769(1)
Cp^{*ethyl}	1.7547(13)	2.3879(10)	2.4439(9)	3.7025(5)
$Cp^{*n\text{-propyl}}$	1.7541(10)	2.3925(7)	2.4486(6)	3.74982(17)
$Cp^{*n\text{-butyl}}$	1.7591(18)	2.3912(10)	2.4518(9)	3.7803(4)
[a]$Cp^{*n\text{-pentyl}}$	1.7579(16)	2.4041(9)	2.4541(9)	3.7371(6)

[a] DCM present in the crystal lattice.

Table 29. Comparison of bond lengths for modified Cp* rings for iridium.

Ligand	Ir-C(centroid)	Ir-Cl (T)	Ir-Cl(bridging)	Ir-Ir
$Cp^{*phenyl}$	1.749	2.3899(7)	2.4378(8)	3.7157(4)
$Cp^{*benzyl}$	1.74621(8)	2.3914(7)	2.4549(7)	3.7107(3)
$Cp^{*phenethyl}$	1.7531(12)	2.3919(8)	2.4567(7)	3.7446(5)

A similar trend can be seen with all angles (**Table 30**). Both angles Ir-Cl-(B)-Ir' and Cl(T)-Ir-Cl(B) increase from Cp^{*ethyl} to $Cp^{*n\text{-butyl}}$ as a result of the increasing distance between the Ir-Ir distance. Consequently, the Cl(B)-Ir-Cl(B)' angle decreases as a result of the increasing distance between each metal. Therefore, the increasing length of the alkyl chain without solvent affects the angles directly. Lastly, analysis of the modified ring iridium dimers reveals little to no difference between the bond angles (**Table 31**).

Table 30. Comparison of bond angles for unmodified and modified Cp* chains for iridium

Ligand	Ir-Cl(B)-Ir'	Cl(B)-Ir-Cl(B)'	Cl(T)-Ir-Cl(B)
Cp*	100.45(12)	79.55(12)	89.65(12)
Cp*^{ethyl}	98.46(3)	81.54(3)	87.86(3)
Cp*$^{n\text{-propyl}}$	100.10(2)	79.90(2)	88.86(2)
Cp*$^{n\text{-butyl}}$	100.63(3)	79.37(3)	89.31(3)
[a]Cp*$^{n\text{-pentyl}}$	99.41(3)	80.59(3)	88.20(3)

[a] DCM present in the crystal lattice.

Table 31. Comparison of bond angles for modified Cp* rings for iridium.

Ligand	Ir-Cl(B)-Ir'	Cl(B)-Ir-Cl(B)'	Cl(T)-Ir-Cl(B)
Cp*^{phenyl}	99.21(3)	80.79(3)	86.79(3)
Cp*^{benzyl}	98.19(4)	81.81(4)	87.73(4)
Cp*^{phenethyl}	99.24(2)	80.77(2)	88.86(3)

In comparison to the iridium trend, the Rh-Rh bond distance experiences a greater variability. There is little to no difference between the Rh-C and the Rh-Cl(bridging) bond distances as the length of the alkyl chain increases. There is a decrease from the Cp* to Cp*^{ethyl} similar to that of iridium. In contrast, the even numbered chain lengths, 2 and 4, have shorter bond lengths than their odd chain length counterparts, 3 and 5. There is a different trend observed for rhodium modified ring Cp*^{R} variants. The Rh-Rh distance increases as the number of methylenes increase (**Table 33**). The rhodium Cp*^{phenyl} does not exhibit any π-π stacking interactions (4.658Å) similar to the one found by Sadler in the iridium Cp*^{phenyl}.[41]

Table 32. Comparison of bond lengths for unmodified and modified Cp* chains for rhodium.

Ligand	Rh-C(centroid)	Rh-Cl (T)	Rh-Cl(bridging)	Rh-Rh
Cp*	1.7558 (3)	2.3967(11)	2.4649(11)	3.7191(6)
Cp*^{ethyl}	1.7566(13)	2.4102(8)	2.4458(7)	3.7024(6)
Cp*$^{n\text{-propyl}}$	1.7586(7)	2.4096(4)	2.4608(4)	3.7192(4)
Cp*$^{n\text{-butyl}}$	1.7511(14)	2.3973(8)	2.4642(8)	3.6174(6)
[a]Cp*$^{n\text{-pentyl}}$	1.7557(9)	2.4102(5)	2.4489(5)	3.6782(6)

[a] DCM present in the crystal lattice.

Table 33. Comparison of bond lengths for modified Cp* rings for rhodium.

Ligand	Rh-C(centroid)	Rh-Cl (T)	Rh-Cl(bridging)	Rh-Rh
Cp*^{phenyl}	1.7540	2.3813(6)	2.4460(6)	3.5980(2)
Cp*^{benzyl}	1.7533(11)	2.3984(6)	2.4553(6)	3.6502(8)
Cp*^{phenethyl}	1.7486(7)	2.3947(4)	2.4586(4)	3.6811(5)

As the Rh-Rh distance fluctuates for the alkyl chains, each angle fluctuates accordingly (**Table 34**). In contrast, the modified Cp* ring Rh-Rh distance increases for each methylene, resulting in both angles, Rh-Cl(B)-Rh' and Cl(T)-Rh-Cl(B), increasing and the Cl(B)-Rh-Cl(B)' decreasing (**Table 35**).

Table 34. Comparison of bond angles for unmodified and modified Cp* chains for rhodium.

Ligand	Rh-Cl(B)-Rh'	Cl(B)-Rh-Cl(B)'	Cl(T)-Rh-Cl(B)
Cp*	98.29(3)	81.71(3)	92.30(4)
Cp*^{ethyl}	97.77(3)	82.51(3)	91.01(3)
Cp*$^{n\text{-propyl}}$	98.405(13)	81.595(13)	92.288(14)
Cp*$^{n\text{-butyl}}$	94.25(3)	85.75(3)	89.62(3)
Cp*$^{n\text{-pentyl}}$	97.123(19)	82.8876(19)	90.832(18)

Table 35. Comparison of bond angles for modified Cp* rings for rhodium.

Ligand	Rh-Cl(B)-Rh'	Cl(B)-Rh-Cl(B)'	Cl(T)-Rh-Cl(B)
Cp*^{phenyl}	94.70(2)	85.30(2)	90.15
Cp*^{benzyl}	95.43(2)	84.568(19)	90.08(2)
Cp*^{phenethyl}	96.811(14)	83.189(14)	91.146(15)

At this time, this is the first complete study of modified Cp*^{R} dimers with two different metals. Each of these modified complexes showed that rhodium and iridium behave similarly in solid state. All crystal structures will provide insight into how the R group can affect steric interactions by the chain length or via bulk interactions of a ring substituent.

3.4 Potential use of modified iridium and rhodium dimers

The efficient synthesis of rhodium and iridium modified pentasubstituted cyclopentadienyl complexes allows for greater opportunities to explore cyclopentadienyl chemistry. Until now, 9 of the modified dimers have been synthesized and subsequently had their yield improved. The other 21 modified dimers allow for a complete comparison of the substituent effect on modified cyclopentadienes with various R groups between iridium and rhodium.

The catalytic formation of lactones is a unique opportunity as it provides valuable intermediates. Lactones can be used in the synthesis of pharmaceuticals, natural products, and ring opening polymerization (ROP). ROP of lactones allows for the creation of ester linkages[47] and biodegradable polymers.[48] Thus far, several lactones have been synthesized from their corresponding diols as seen in **Figure 36** and **Table 36**. Optimization of this catalytic system followed by rate of reaction, turnover frequency (TON), and yield will be studied using gas chromatography.

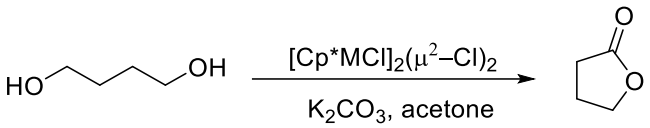

Figure 36. General schematic for the oxidative lactonization of diols catalyzed by $[Cp^{*R}MCl]_2(\mu^2\text{-}Cl)_2$ (M = Rh, Ir).

Table 36. Oxidative lactonization of diols catalyzed by an iridium or rhodium catalyst.[a]

Entry	Diol	Product
1	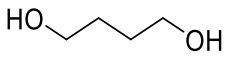	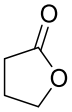
2	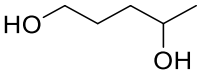	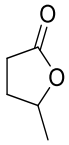
3	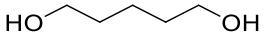	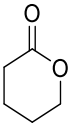
4	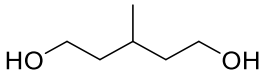	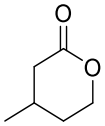
5	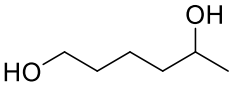	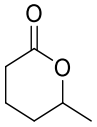
6	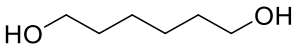	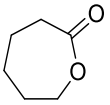
7	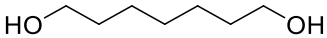	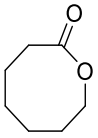

[a] Unless otherwise stated, the reaction was carried out at room temperature using a 1.0 M solution of diol (1.0 mmol) in acetone. Diol/C (C = catalyst) = 200:1.

Oxidation of diols with varied substituents on the chains will lead to the formation of chiral lactones; diols with fluorinated chains are of particular interest. Fluorinated lactones can lead to a variety of fluoropolymers and fluorosurfactants. This pathway is of significant interest as ROP of fluorinated lactones will provide a synthetic route for fluoropolymers.

In addition to the diol catalytic study, the use of modified dimers will be used in the dimerization of alcohols using a Guerbet reaction (**Figure 37**, **Figure 38**). Phenethyl alcohol will be a starting point of the catalytic study as it has been shown to exhibit antimicrobial activity.[49] As this alcohol has been rarely studied, this opens up potential for greater exploration with derivatives

of phenethyl alcohol. The number and location of phenyl substituents has been shown to affect biological activity as Sadler has demonstrated[7a] as well as the Merola group. Therefore, the dimerization of phenethyl alcohol is appealing as it can lead to the development of an effective anti-microbial agent.

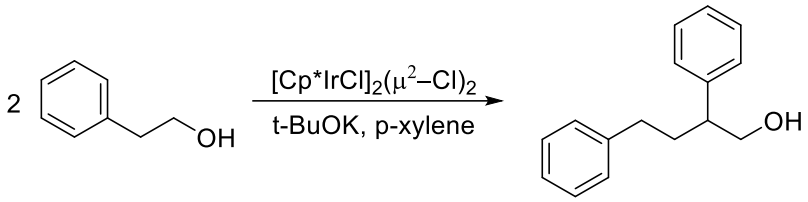

Figure 37. General schematic for the Guerbet reaction of phenethyl alcohol catalyzed by $[Cp^*IrCl]_2(\mu^2\text{-}Cl)_2$.

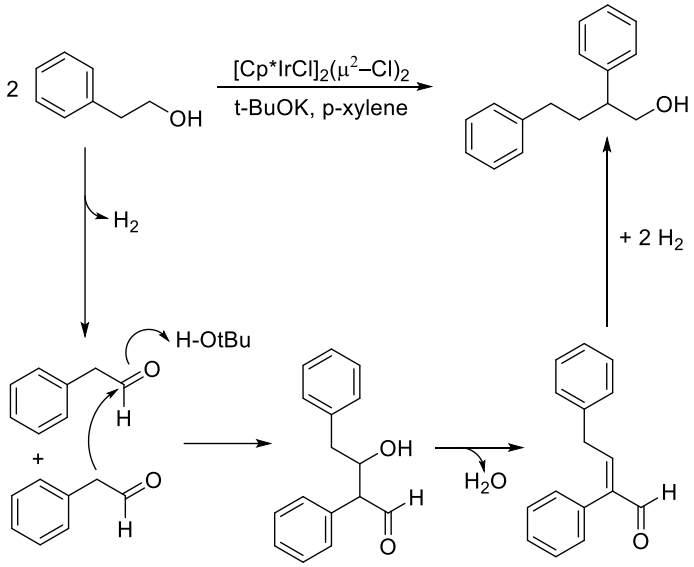

Figure 38. Mechanistic schematic for the Guerbet reaction of phenethyl alcohol catalyzed by $[Cp^*IrCl]_2(\mu^2\text{-}Cl)_2$.

The application of modified Cp^{*R} dimers will assist in the synthesis of half-sandwich complexes tailored for catalytic activity or biological activity. Just as Suzuki successfully used the amino alcohol complex $Cp^*IrCl[OCH_2C(C_6H_5)_2NH_2]$ for a variety of transfer hydrogenation systems,[17, 20, 50] the use of the modified catalysts in multiple catalytic systems shows noteworthy

potential. Thus far, the amino acid complex Cp*IrCl[O(CO)C(C_6H_5)$_2$$NH_2$] has shown catalytic activity in the formation of lactones from diols. The alternative to the expensive amino alcohol ($450/g) is diphenylglycine as it only costs $23.2/g. This complex is unique as it has an open site for coordination, allowing substrates to bind to the metal.

Chapter 4 Conclusion and Future Work

An extensive library of iridium and rhodium dimeric complexes of the form $[(\eta^5\text{-ring})MCl]_2(\mu^2\text{-Cl})_2$ were synthesized and characterized. Pentasubstituted cyclopentadienyl ligands were synthesized by reaction with their respective Grignard reagent and 2,3,4,5-tetramethylcyclopent-2-en-1-one. The modified HCp*R ligands were reacted with $[M(COD)]_2(\mu^2\text{-Cl})_2$ (M = Ir, Rh) to produce the dimeric compounds in yields ranging from 16% - 96%. The use of a microwave reactor reduced reaction times from 48 hours to 1 hour and increased yields for all of the dimeric complexes. This library of compounds will not only enhance the research efforts of the Merola group, instead will be of use to a large number of researchers investigating the catalytic and biological activity of compounds using the library of dimers as starting materials.

Crystal structures of these complexes showed that most of the iridium and rhodium dimers were isostructural. Pentasubstituted cyclopentadienyl dimers $[Cp^{*R}MCl]_2(\mu^2\text{-Cl})_2$ (M = Ir(III), Rh(III)) follow the 18 electron rule per metal center, for a total of 36 electrons per dimer. Each of these compounds contains two bridging chlorides between the metals and were found to belong to the monoclinic space group No. 14 ($P2_1/c$) with the exception of the *n*-butyl dimers. While no clear electronic or other trends could be clearly discerned from the single crystal X-ray diffraction studies, nonetheless this library of crystallographic information may still prove to be valuable once catalytic and biological activity information is determined and compared with the X-ray data.

In summary, this work has shown that a modular catalyst design is possible by using a microwave reactor. The simple modification of HCp^{*R} ligands has great potential as evidenced by their use with pentamethylcyclopentadiene. These modified dimeric species are being explored further in ring closure catalysis such as amino alcohols to lactams, diols to lactones, as well as Guerbet type reactions. Preliminary results have shown that both $[Cp^{*R}IrCl]_2(\mu^2\text{-Cl})_2$ and

$[Cp^{*R}RhCl]_2(\mu^2\text{-}Cl)_2$ catalyze diols into their corresponding lactones. This occurrence shows that the diols undergo a similar mechanism with $[Cp^{*R}MCl]_2(\mu^2\text{-}Cl)_2$ (M = Ir(III), Rh(III)) than $Cp^*IrCl[OCH_2(C_6H_5)_2NH_2]$ examined by Suzuki. Further catalytic and identification studies via GC-MS will assist in determining the product.

In addition to potential catalytic activities, the chemotherapeutic and anti-microbial properties of these dimers and their subsequently produced half-sandwich complexes are being investigated. Lastly, this methodology will be adapted for use with a more powerful microwave in hopes of synthesizing these dimers with a reaction time of less than 5 minutes.

REFERENCES

1. Chen, S.-j.; Lu, G.-p.; Cai, C., A base-controlled chemoselective transfer hydrogenation of α,β-unsaturated ketones catalyzed by $[IrCp^*Cl_2]_2$ with 2-propanol. *RSC Advances* **2015,** *5* (17), 13208-13211.
2. Gunay, A.; Mantell, M. A.; Field, K. D.; Wu, W.; Chin, M.; Emmert, M. H., Oxidation catalysis in air with Cp*Ir: influence of added ligands and reaction conditions on catalytic activity and stability. *Catal. Sci. Technol.* **2015,** *5* (2), 1198-1205.
3. Liu, J.; Wu, X.; Iggo, J. A.; Xiao, J., Half-sandwich iridium complexes—Synthesis and applications in catalysis. *Coordination Chemistry Reviews* **2008,** *252* (5-7), 782-809.
4. White, C.; Yates, A.; Maitlis, P. M.; Heinekey, D. M., (η^5-Pentamethylcyclopentadienyl)Rhodium and -Iridium Compounds. In *Inorganic Syntheses*, John Wiley & Sons, Inc.: 2007; pp 228-234.
5. Cuenca, T.; Royo, P., Transition metal complexes with functionalized silyl-substituted cyclopentadienyl and related ligands: synthesis and reactivity. *Coordination Chemistry Reviews* **1999,** *193–195*, 447-498.
6. Morris, D. M.; McGeagh, M.; De Peña, D.; Merola, J. S., Extending the range of pentasubstituted cyclopentadienyl compounds: The synthesis of a series of tetramethyl(alkyl or aryl)cyclopentadienes (Cp∗R), their iridium complexes and their catalytic activity for asymmetric transfer hydrogenation. *Polyhedron* **2014,** *84*, 120-135.
7. (a) Liu, Z.; Habtemariam, A.; Pizarro, A. M.; Fletcher, S. A.; Kisova, A.; Vrana, O.; Salassa, L.; Bruijnincx, P. C.; Clarkson, G. J.; Brabec, V.; Sadler, P. J., Organometallic half-sandwich iridium anticancer complexes. *J Med Chem* **2011,** *54* (8), 3011-26; (b) Dooley, T.; Fairhurst, G.; Chalk, C. D.; Tabatabaian, K.; White, C., Ethyltetramethylcyclopentadienyl complexes of cobalt, rhodium, iridium and ruthenium. *Transition Metal Chemistry 3* (1), 299-302.
8. (a) Fujita, K.-i.; Li, Z.; Ozeki, N.; Yamaguchi, R., N-Alkylation of amines with alcohols catalyzed by a Cp*Ir complex. *Tetrahedron Letters* **2003,** *44* (13), 2687-2690; (b) Kawahara, R.; Fujita, K.-i.; Yamaguchi, R., N-Alkylation of Amines with Alcohols Catalyzed by a Water-Soluble Cp*Iridium Complex: An Efficient Method for the Synthesis of Amines in Aqueous Media. *Advanced Synthesis & Catalysis* **2011,** *353* (7), 1161-1168; (c) Saidi, O.; Blacker, A. J.; Farah, M. M.; Marsden, S. P.; Williams, J. M. J., Iridium-catalysed amine alkylation with alcohols in water. *Chemical Communications* **2010,** *46* (9), 1541-1543.
9. Fujita, K.-i.; Fujii, T.; Yamaguchi, R., Cp*Ir Complex-Catalyzed N-Heterocyclization of Primary Amines with Diols: A New Catalytic System for Environmentally Benign Synthesis of Cyclic Amines. *Organic Letters* **2004,** *6* (20), 3525-3528.
10. Xia, Y.; Liu, Z.; Feng, S.; Zhang, Y.; Wang, J., Ir(III)-Catalyzed Aromatic C–H Bond Functionalization via Metal Carbene Migratory Insertion. *The Journal of Organic Chemistry* **2015,** *80* (1), 223-236.
11. Kumaran, E.; Leong, W. K., $[Cp^*RhCl_2]_2$-Catalyzed Alkyne Hydroamination to 1,2-Dihydroquinolines. *Organometallics* **2015,** *34* (9), 1779-1782.
12. (a) Suzuki, T.; Morita, K.; Matsuo, Y.; Hiroi, K., Catalytic asymmetric oxidative lactonizations of meso-diols using a chiral iridium complex. *Tetrahedron Letters* **2003,** *44* (10), 2003-2006; (b) Hamada, T.; Torii, T.; Izawa, K.; Ikariya, T., A practical synthesis of optically active aromatic epoxides via asymmetric transfer hydrogenation of α-chlorinated ketones with chiral rhodium–diamine catalyst. *Tetrahedron* **2004,** *60* (34), 7411-7417; (c) Saidi, O.; Bamford, M. J.; Blacker, A. J.; Lynch, J.; Marsden, S. P.; Plucinski, P.; Watson, R. J.; Williams, J. M. J., Iridium-catalyzed formylation of amines with paraformaldehyde. *Tetrahedron Letters* **2010,** *51*

(44), 5804-5806; (d) Hatanaka, S.; Obora, Y.; Ishii, Y., Iridium-Catalyzed Coupling Reaction of Primary Alcohols with 2-Alkynes Leading to Hydroacylation Products. *Chemistry – A European Journal* **2010,** *16* (6), 1883-1888; (e) Iuchi, Y.; Obora, Y.; Ishii, Y., Iridium-Catalyzed α-Alkylation of Acetates with Primary Alcohols and Diols. *Journal of the American Chemical Society* **2010,** *132* (8), 2536-2537; (f) Izumi, A.; Obora, Y.; Sakaguchi, S.; Ishii, Y., Oxidative dimerization of primary alcohols to esters catalyzed by iridium complexes. *Tetrahedron Letters* **2006,** *47* (52), 9199-9201; (g) Koda, K.; Matsu-ura, T.; Obora, Y.; Ishii, Y., Guerbet Reaction of Ethanol to n-Butanol Catalyzed by Iridium Complexes. *Chemistry Letters* **2009,** *38* (8), 838-839; (h) Matsu-ura, T.; Sakaguchi, S.; Obora, Y.; Ishii, Y., Guerbet Reaction of Primary Alcohols Leading to β-Alkylated Dimer Alcohols Catalyzed by Iridium Complexes. *The Journal of Organic Chemistry* **2006,** *71* (21), 8306-8308.

13. Fujita, K.-i.; Furukawa, S.; Yamaguchi, R., Oxidation of primary and secondary alcohols catalyzed by a pentamethylcyclopentadienyliridium complex. *Journal of Organometallic Chemistry* **2002,** *649* (2), 289-292.

14. Fujita, K.-i.; Kitatsuji, C.; Furukawa, S.; Yamaguchi, R., Regio- and chemoselective transfer hydrogenation of quinolines catalyzed by a Cp*Ir complex. *Tetrahedron Letters* **2004,** *45* (16), 3215-3217.

15. Katritzky, A. R.; Rachwal, S.; Rachwal, B., Recent progress in the synthesis of 1,2,3,4,-tetrahydroquinolines. *Tetrahedron* **1996,** *52* (48), 15031-15070.

16. Fujita, K.-i.; Takahashi, Y.; Owaki, M.; Yamamoto, K.; Yamaguchi, R., Synthesis of Five-, Six-, and Seven-Membered Ring Lactams by Cp*Rh Complex-Catalyzed Oxidative N-Heterocyclization of Amino Alcohols. *Organic Letters* **2004,** *6* (16), 2785-2788.

17. Suzuki, T.; Morita, K.; Tsuchida, M.; Hiroi, K., Iridium-Catalyzed Oppenauer Oxidations of Primary Alcohols Using Acetone or 2-Butanone as Oxidant. *The Journal of Organic Chemistry* **2003,** *68* (4), 1601-1602.

18. Karpin, G. W.; Merola, J. S.; Falkinham, J. O., 3rd, Transition metal-alpha-amino acid complexes with antibiotic activity against Mycobacterium spp. *Antimicrob Agents Chemother* **2013,** *57* (7), 3434-6.

19. Millett, A. J.; Habtemariam, A.; Romero-Canelón, I.; Clarkson, G. J.; Sadler, P. J., Contrasting Anticancer Activity of Half-Sandwich Iridium(III) Complexes Bearing Functionally Diverse 2-Phenylpyridine Ligands. *Organometallics* **2015,** *34* (11), 2683-2694.

20. Suzuki, T.; Morita, K.; Tsuchida, M.; Hiroi, K., Mild and Chemoselective Synthesis of Lactones from Diols Using a Novel Metal−Ligand Bifunctional Catalyst. *Organic Letters* **2002,** *4* (14), 2361-2363.

21. Śliwińska, U.; Pruchnik, F. P.; Ułaszewski, S.; Latocha, M.; Nawrocka-Musiał, D., Properties of η^5-pentamethylcyclopentadienyl rhodium(III) and iridium(III) complexes with quinolin-8-ol and their cytostatic activity. *Polyhedron* **2010,** *29* (6), 1653-1659.

22. Baghurst, D. R.; Michael, D.; Mingos, P.; Watson, M. J., Application of microwave dielectric loss heating effects for the rapid and convenient synthesis of organometallic compounds. *Journal of Organometallic Chemistry* **1989,** *368* (3), C43-C45.

23. Baghurst, D. R.; Cooper, S. R.; Greene, D. L.; Mingos, D. M. P.; Reynolds, S. M., Application of microwave dielectric loss heating effects for the rapid and convenient synthesis of coordination compounds. *Polyhedron* **1990,** *9* (6), 893-895.

24. Strauss, C.; Trainor, R., Developments in Microwave-Assisted Organic Chemistry. *Australian Journal of Chemistry* **1995,** *48* (10), 1665-1692.

25. Larhed, M.; Hallberg, A., Microwave-assisted high-speed chemistry: a new technique in drug discovery. *Drug Discovery Today* **2001,** *6* (8), 406-416.
26. Lidström, P.; Tierney, J.; Wathey, B.; Westman, J., Microwave assisted organic synthesis—a review. *Tetrahedron* **2001,** *57* (45), 9225-9283.
27. Moseley, J. D.; Kappe, C. O., A critical assessment of the greenness and energy efficiency of microwave-assisted organic synthesis. *Green Chemistry* **2011,** *13* (4), 794-806.
28. Gabriel, C.; Gabriel, S.; H. Grant, E.; H. Grant, E.; S. J. Halstead, B.; Michael P. Mingos, D., Dielectric parameters relevant to microwave dielectric heating. *Chemical Society Reviews* **1998,** *27* (3), 213-224.
29. Baghurst, D. R.; Mingos, D. M. P., Design and application of a reflux modification for the synthesis of organometallic compounds using microwave dielectric loss heating effects. *Journal of Organometallic Chemistry* **1990,** *384* (3), C57-C60.
30. Gedye, R.; Smith, F.; Westaway, K.; Ali, H.; Baldisera, L.; Laberge, L.; Rousell, J., The use of microwave ovens for rapid organic synthesis. *Tetrahedron Letters* **1986,** *27* (3), 279-282.
31. (a) Schmidlehner, M.; Kuhn, P.-S.; Hackl, C. M.; Roller, A.; Kandioller, W.; Keppler, B. K., Microwave-assisted synthesis of N-heterocycle-based organometallics. *Journal of Organometallic Chemistry* **2014,** *772-773*, 93-99; (b) Tönnemann, J.; Risse, J.; Grote, Z.; Scopelliti, R.; Severin, K., Efficient and Rapid Synthesis of Chlorido-Bridged Half-Sandwich Complexes of Ruthenium, Rhodium, and Iridium by Microwave Heating. *European Journal of Inorganic Chemistry* **2013,** *2013* (26), 4558-4562.
32. (a) Strauss, C. R., Microwave-Assisted Reactions in Organic Synthesis—Are There Any Nonthermal Microwave Effects? Response to the Highlight by N. Kuhnert. *Angewandte Chemie* **2002,** *114* (19), 3741-3743; (b) Dudley, G. B.; Richert, R.; Stiegman, A. E., On the existence of and mechanism for microwave-specific reaction rate enhancement. *Chemical Science* **2015,** *6* (4), 2144-2152; (c) Kappe, C. O.; Stadler, A., Microwave Theory. In *Microwaves in Organic and Medicinal Chemistry*, Wiley-VCH Verlag GmbH & Co. KGaA: 2006; pp 9-28.
33. (a) Kappe, C. O.; Dallinger, D.; Murphree, S. S., Microwave Theory. In *Practical Microwave Synthesis for Organic Chemists*, Wiley-VCH Verlag GmbH & Co. KGaA: 2009; pp 11-44; (b) Kappe, C. O.; Pieber, B.; Dallinger, D., Microwave Effects in Organic Synthesis: Myth or Reality? *Angewandte Chemie International Edition* **2013,** *52* (4), 1088-1094.
34. de la Hoz, A.; Diaz-Ortiz, A.; Moreno, A., Microwaves in organic synthesis. Thermal and non-thermal microwave effects. *Chemical Society Reviews* **2005,** *34* (2), 164-178.
35. C. Oliver Kappe, D. D., Shaun S. Murphree, *Practical Microwave Synthesis for Organic Chemists*. 2009.
36. El Amouri, H.; Gruselle, M.; Jaouén, G., bis[Dichloro(η-pentamethylcyclopentadienyl)rhodium(III) and -iridium(III)] from bis[Chloro(1, 5-cyclooctadiene)rhodium(I) and -iridium(I)] Oxidation, and Formation of 1, 5-Cyclooctadiene(η-pentamethylcyclopentadienyl)rhodium(I). *Synthesis and Reactivity in Inorganic and Metal-Organic Chemistry* **1994,** *24* (3), 395-400.
37. Jutzi, P., The Versatility of the Pentamethylcyclopentadienyl Ligand in Main-Group Chemistry. *Comments on Inorganic Chemistry* **1987,** *6* (3), 123-144.
38. (a) Pinkas, J.; Lamač, M., Transformations of functional groups attached to cyclopentadienyl or related ligands in group 4 metal complexes. *Coordination Chemistry Reviews* **2015,** *296*, 45-90; (b) Coville, N. J.; du Plooy, K. E.; Pickl, W., Monosubstituted cyclopentadienyl half-sandwich transition metal complexes. *Coordination Chemistry Reviews* **1992,** *116*, 1-267.

39. Lucas, S. J.; Lord, R. M.; Basri, A. M.; Allison, S. A.; Phillips, R. M.; Blacker, J.; McGowan, P. C., Increasing Anti-Cancer Activity with Longer Tether Lengths of Group 9 Cp* Complexes. *Dalton Transactions* **2016**.
40. Li, J.; Tang, Y.; Wang, Q.; Li, X.; Cun, L.; Zhang, X.; Zhu, J.; Li, L.; Deng, J., Chiral Surfactant-Type Catalyst for Asymmetric Reduction of Aliphatic Ketones in Water. *Journal of the American Chemical Society* **2012,** *134* (45), 18522-18525.
41. Miyano, Y.; Nakai, H.; Hayashi, Y.; Isobe, K., Synthesis and structural characterization of a photoresponsive organodirhodium complex with active S–S bonds: $[(CpPhRh)_2(\mu\text{-}CH_2)_2(\mu\text{-}O_2SSO_2)]$ ($CpPh=\eta^5\text{-}C_5Me_4Ph$). *Journal of Organometallic Chemistry* **2007,** *692* (1-3), 122-128.
42. Morris, D. M. Design and Modficiation of Half-Sandwich Ir(III), Rh(III), and Ru(II) Amino Acid Complexes for Application in Asymmetric Transfer Hydrogenation Reactions. Dissertation, Virginia Polytechnic Institute and State University, 2015.
43. El Amouri, H.; Gruselle, M.; Jaouén, G., bis[Dichloro(η-pentamethylcyclopentadienyl)rhodium(III) and -iridium(III)] frombis[Chloro(1, 5-cyclooctadiene)rhodium(I) and -iridium(I)] Oxidation, and Formation of 1, 5-Cyclooctadiene(η-pentamethylcyclopentadienyl)rhodium(I). *Synthesis and Reactivity in Inorganic and Metal-Organic Chemistry* **1994,** *24* (3), 395-400.
44. (a) Churchill, M. R.; Julis, S. A.; Rotella, F. J., Comparative geometry of $Rh(\mu\text{-}Cl)_2Rh$ and $Rh(\mu\text{-}H)(\mu\text{-}Cl)Rh$ Bridges. Crystal structure of $[\eta^5\text{-}C_5Me_5RhCl]_2(\mu\text{-}Cl)_2$ and its relationship to $[\eta^5\text{-}C_5Me_5RhCl]_2(\mu\text{-}H)(\mu\text{-}Cl)$. *Inorganic Chemistry* **1977,** *16* (5), 1137-1141; (b) Churchill, M. R.; Julis, S. A., Crystal structure and molecular geometry of homogeneous hydrogenation catalyst $[\eta^5\text{-}C_5Me_5RhCl]_2(\mu\text{-}H)(\mu\text{-}Cl)$ and of its precursor $[\eta^5\text{-}C_5Me_5RhCl]_2(\mu\text{-}Cl)_2$. A direct comparison of $Ir(\mu\text{-}H)(\mu\text{-}Cl)Ir$ and $Ir(\mu\text{-}Cl)_2Ir$ bridging systems. *Inorganic Chemistry* **1977,** *16* (6), 1488-1494.
45. Abramov, P. A.; Sokolov, M. N.; Virovets, A. V.; Fedin, V. P., Crystal structure of $[(C_5Me_4Et)_3Rh_3(\mu^3\text{-}Se)_2](PF_6)_2CH_3CN$ and $[(C_5Me_4Et)_2Rh_2(\mu^2\text{-}Cl)_3]PF_6$. *J Struct Chem* **2009,** *50* (1), 162-165.
46. Merola, J. S.; Morris, D.; De Weerd, N., Di-μ2-chlorido-bis-[chlorido(η^5-2,3,4,5-tetramethyl-1-propylcyclopentadienyl)iridium(III)]. *Acta Crystallogr Sect E Struct Rep Online* **2013,** *69* (Pt 3), m176.
47. Nishiura, M.; Hou, Z.; Koizumi, T.-a.; Imamoto, T.; Wakatsuki, Y., Ring-Opening Polymerization and Copolymerization of Lactones by Samarium(II) Aryloxide Complexes. *Macromolecules* **1999,** *32* (25), 8245-8251.
48. (a) Chen, T.; Qin, Z.; Qi, Y.; Deng, T.; Ge, X.; Wang, J.; Hou, X., Degradable polymers from ring-opening polymerization of α-angelica lactone, a five-membered unsaturated lactone. *Polymer Chemistry* **2011,** *2* (5), 1190-1194; (b) Wang, Y.-L.; Zhou, Y.-X.; Deng, L.-Q.; Hu, Q.-S.; Tao, X.; Shen, Y.-Z., Synthesis and structure characterization of bis- and mono(amidate) lanthanide (Ln = La, Gd) complexes and their application in the polymerization of ε-caprolactone. *Journal of Organometallic Chemistry* **2016,** *805*, 77-86; (c) Hsiao, H.-C.; Datta, A.; Chen, Y.-F.; Chang, W.; Lee, T.-Y.; Lin, C.-H.; Huang, J.-H., Structural aspects and ring opening polymerization of ε-caprolactone using mono- and di-aluminum compounds incorporating bidentate pyrrole-morpholine ligands. *Journal of Organometallic Chemistry* **2016,** *804*, 35-41.
49. Lingappa, B. T.; Prasad, M.; Lingappa, Y.; Hunt, D. F.; Biemann, K., Phenethyl Alcohol and Tryptophol: Autoantibiotics Produced by the Fungus Candida albicans. *Science* **1969,** *163* (3863), 192-194.

50. Suzuki, T.; Yamada, T.; Watanabe, K.; Katoh, T., Iridium-catalyzed oxidative lactonization and intramolecular Tishchenko reaction of δ-ketoaldehydes for the synthesis of isocoumarins and 3,4-dihydroisocoumarins. *Bioorg Med Chem Lett* **2005,** *15* (10), 2583-5.